공학박사 학위논문

The fabrication and electrochemical analysis of Pt-free counter electrodes for dye-sensitized solar cells

비백금 염료감응형 태양전지 상대 전극의 제조와 전기화학 분석

2013 년 2 월

서울대학교 대학원

화학생물공학부

박 선 하

The fabrication and electrochemical analysis of Pt-free counter electrodes for dye-sensitized solar cells

지도교수 성 영 은

이 논문을 공학박사 학위논문으로 제출함
2012 년 12 월

서울대학교 대학원
화학생물공학부
박 선 하

박선하의 공학박사 학위논문을 인준함
2012 년 12 월

위 원 장 오 승모 (인)
부위원장 성 영은 (인)
위 원 김 대형 (인)
위 원 최 희만 (인)
위 원 안 광순 (인)

Abstract

The fabrication and electrochemical analysis of Pt-free counter electrodes for dye-sensitized solar cells

Sun Ha Park

School of Chemical and Biological Engineering

The Graduate School

Seoul National University

In this paper, four different low-cost materials were applied as a Pt-free or Pt and TCO-free counter electrodes for dye-sensitized solar cell (DSSC). To replace conventional platinum (Pt) coated transparent conducting oxide (TCO) electrode, materials for counter electrode require high catalytic activity for I_3^- reduction and rapid charge transport ability.

Firstly, the well-ordered inverse opal poly(3,4-ethylenedioxythiophene) (PEDOT) electrode which was prepared from PEDOT:PSS filled self-assembled PS opal template was applied as a Pt-free counter electrode for DSSC. Because of the well-ordered porous morphology of electrode, the inverse opal structured PEDOT electrode showed, in particular, improved electrocatalytic activity with high surface area and the increased quantum efficiency at specific wavelength was also observed particularly. Therefore,

we could successfully apply the inverse opal structured PEDOT electrode as an effective Pt-free counter electrode for DSSCs. Furthermore, the Ni nitrides, which are known for a high electrocatalytic activity in iodide redox couple, were deposited on the ITO/PET film by sputtering deposition at low-temperature and could be also used as Pt-free flexible counter electrode for DSSC. By sputtering under nitrogen atmosphere at different temperature, a few nano-meter Ni nitride film was deposited on ITO/PET films and exhibited superior electrocatalytic activities in iodide redox electrolyte. In addition, this Ni nitride film had very thin thicknesses, about 30 nm, on the flexible ITO/PET substrate, it could be applied as a counter electrode for bifacial DSSC due to the optical transparency of Ni nitride film.

On the other hand, Pt and TCO-free counter electrode was also studied to realize the cost effective counter electrode for DSSC. We found the two materials which functioned two things, high catalytic activity for triiodide reduction and high conductivity rapidly transporting the electron, in a single layer simultaneously. The nitrided Ni metal foam electrode was applied as a Pt and TCO-free counter electrode of DSSC for the first time. The nitrided Ni foam was simple synthesized by nitridation treatment of commercial Ni metal foam in ammonia atmosphere. This electrode was presented high catalytic activity on the nitrided surface and easy electron transport ability in the three-dimensional interconnected metallic structure, simultaneously. The open-pore structures in metal foam can also reduce the mass transport limitations of the electrolyte in the electrode compared to that of common metal plate. Therefore, the nitrided Ni foam using nitridation treatment under ammonia atmosphere can be a new

cost-efficient counter electrode without the expensive Pt and TCO commonly used in counter electrode of DSSC. Lastly, the camphorsulfonic acid-doped polyaniline (PANI/CSA) electrode was prepared by simple spin-coating deposition flowed by low-temperature treatment was successfully used as a Pt and TCO-free counter electrode for DSSC. The PANI/CSA is a well-known conducting polymer with high conductivity and it provided excellent electrocatalytic ability because π-conjugated polymer superseded Pt as efficient electrocatalyst for iodide reduction reactions. By several optimization process of PANI/CSA electrode, it could be used as a promising Pt and TCO-free counter electrode of DSSC. Because this electrode had optical transparency and complementary color with dye, it can be used as an effective bifacial DSSC with Pt and TCO-free counter electrode.

Keywords: Dye-sensitized solar cell (DSSC), Pt-free counter electrode, Pt nd TCO-free counter electrode, π-conjugated conducting polymer, nickel nitride.

Student Number: 2009-30242

Contents

List of Tables

List of Figures

Chapter 1. Introduction

1.1 Solar energy and solar cells

The energy that needs for the human is gradually increased, and is likely to double within the near future. Thus, the new energy generation methods which can cover the substantial deficit left by fossil fuels have to be developed. Furthermore, the development of new energy generation methods are promoted by increasing public awareness that the oil price has been raising due to earth's oil could run out during this century. Many researchers have been interested in efficient alternative energy conversion such as solar cells, fuel cells, wind power, geothermal power, and so on.

Because people concern has been concerned about the disastrous environmental pollution arising from all-too-frequent oil spills and the frightening a green-house effect caused by fossil fuel combustion, the photovoltaics have been greatly attracted. The using solar energy has some benefits: the solar energy is sufficient which 10,000 times more than the global population currently consumes and eco-friendly energy sources that does not cause any environmental pollution. For more than two centuries, many researcher sand engineers have been dreamed to realize the idea for photovoltaics which are converting unlimited sunlight into useful electric power or chemical fuels. The most well-known idea to capture the energy from sunlight is the solar cells.[1,2] They are classified as three generations. The silicon based solar cells operated by solid-state junction between two different doped forms of crystalline silicon are the first generation solar cells. It was firstly developed by Bell Telephone Laboratories in 1954, and most widely used in PV markets in these days. To reduce

expensive cost of crystalline silicon solar cells, the thin film solar cells, second generation solar cell, are made from the compound semiconductors, the III/IV aerospace components or the copper-indium-sulphide/selenide material thin films. They also operated by p-n junction technology and show high conversion efficiency in spite of low fabrication cost.[1,3] Recently, the new solar cell called third generation solar cells are focused on many researchers and industries. Their operation mechanism is not a traditional p-n junction but a photoelectrochemical reaction. The semi-conductor nano-materials and conducting polymer were used as elements of solar cells and fabrication process are relatively cheap because the expensive and high-vacuum processes needed for the traditional devices can be avoided. In additions, these solar cells can be used on flexible substrates, and can be shaped or tinted to suit domestic devices or architectural or decorative applications. The developments of research-scaled solar cells from 1970s were depicted in Figure 1.1.

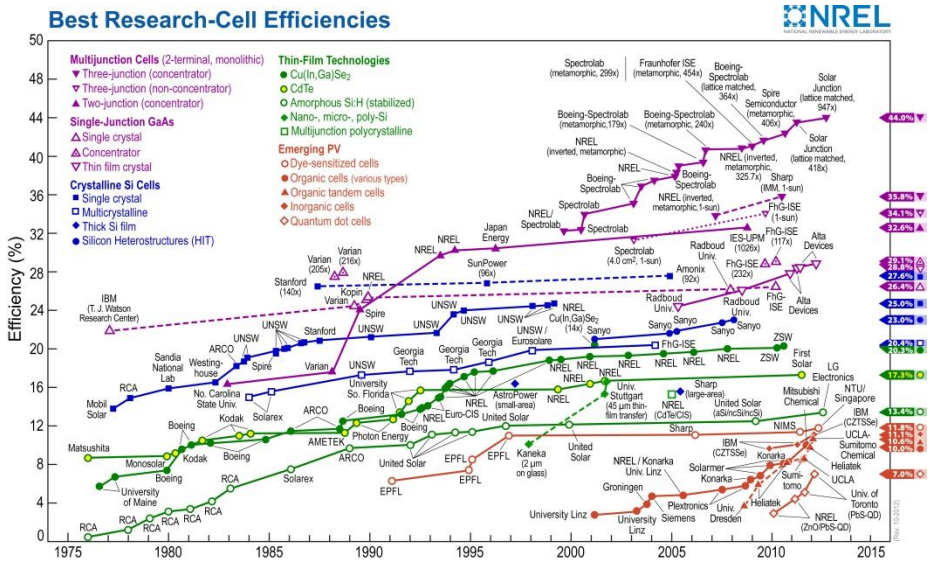

Figure 1.1. Best research-cell efficiencies of solar cells.

(ref. http:// www.nrel.gov/ncpv)

1.2 Dye-sensitized solar cell (DSSCs)

Since Gratzel and O'Regan[2] were reported 7.12 % DSSCs using nanometer sized TiO_2 particles in 1991[1], the dye-sensitized solar cells (DSSCs) have been intensively interested in many researchers and companies because of their low production cost, eco-friendly materials, and solar-to-electrical energy conversion efficiencies as high as 12 %.[4] DSSCs can generate energy with low cost because the components of DSSCs are consisted to abundant materials and fabrication process was very simple and cheap compared to other-type solar cell device. In additions, diverse applications are expected since the DSSCs show colorful characteristics and flexibility

1.2.1 Components of DSSCs

DSSCs have typically been prepared by sandwiching two electrodes, where the photoanode is composed of dye-coated nanocrystalline TiO_2 film deposited on a transparent conducting oxide (TCO), such as FTO (F-doped SnO_2), and the cathode electrode consists of nanoparticle platinum (Pt) on a TCO glass. The TCO substrate acts as a charge collector in DSSC.[1]

The semiconductor structure, typically 10 ㎛ thick and with a porosity of 50%, has a surface area available for dye chemisorption over a thousand times that of a flat, unstructured electrode of the same size. Among the materials for solar cells as presented in Figure 1.2., the semiconductor such as TiO_2, ZnO, SnO_2, Nb_2O_5, etc. can be generally used as photoanodes materials in DSSCs, and the TiO_2 is the most efficient photoanode of DSSCs. To absorbed visible light and then inject electron into the conduction band of the TiO_2, dye molecules anchored to the surface of nanocrystalline TiO_2.[5,6] The dye is chemisorbed as a monomolecular layer, enough can be retained on a given area of

electrode to provide absorption of essentially all the incident light. Over the last 20 years, ruthenium (Ru) complexes have exhibited remarkable efficiency and stability in DSSCs. Recently, the synthesis of transition-metal dye or metal-free organic sensitizer for DSSCs sensitizers has received much attention[7,8], and propylene dye reported highest efficiency in Grätzel group[4].

The cathode, typically called as a counter electrode, is made up of a platinized counter electrode. The counter electrode is one of the major components of the cell and reduces the tri-iodide ions generated after dye regeneration.[9] Since transparent conductive oxide (TCO) substrates exhibit insufficient electron-transfer kinetics for reduction, electrocatalytic layers are coated onto the TCO substrate and used to catalyze the cathodic reduction of tri-iodide ions and regenerate the oxidized redox couple successively. The platinum deposited TCO substrate, In-doped SnO_2 or F-doped SnO_2, electrode was commonly used as a counter electrode for DSSC.

The electrolyte is responsible for charge transport between the photoanode and the counter electrode, the main function of electrolyte is regenerating oxidized dye. The liquid electrolytes with the iodide redox couple and volatile organic solvents were typically used for a long times. However, the iodide redox couple easily corrodes most metals, which shortens the lifetime of commercial modules, and it exhibits poor performances with many alternative dyes other than Ru dyes. Thus, many attempts have been made to solve the above problems by replacing various redox couples. Cobalt complexes, among various redox couples, have recently been proven successful alternative to the iodide redox couple,[10-12] and DSSC using these redox couple was shown the highest conversion efficiency more than 12 %.[4]

1.2.2 Principle of dye sensitized solar cells

The schematic presentation of the operating principles of the DSC is given in Figure 1.3. At the heart of the system is a mesoscopic semiconductor oxide film, which is placed in contact with a redox electrolyte or an organic hole conductor.[6] From the dye attached to the surface of the nanocrystalline TiO_2, photoexcitation was occurred by absorbing the light. And then, the resulted excitation electron is injected into the conduction band of the oxide. The dye is regenerated by electron donation from the electrolyte, usually an organic solvent containing a redox system, such as I^-/I_3^- or Co^{2+}/Co^{3+}. The regeneration of the sensitizer by iodide intercepts the recapture of the conduction band electron by the oxidized dye. The iodide is regenerated, in turn, by the reduction of triiodide at the counter electrode, with the circuit being completed via electron migration through the external load. The voltage generated under illumination corresponds to the difference between the Fermi level of the electron in the solid and the redox potential of the electrolyte. Overall, the device generates electric power from light without suffering any permanent chemical transformation.[13]

1.1.3 Alternative counter electrode

Although the constituents of DSSCs are inexpensive, the counter electrode which transfers electrons from an external circuit to the triiodide and reduces the tri-iodide ions is typically made of platinum (Pt) materials.[14,15] However, Pt is a high cost noble metal with very high cost, thus many efforts have been made to find alternative counter electrode materials to achieve low-cost DSSCs such as Figure 1.4. Several groups have researched replacing Pt counter electrodes with various conducting polymer materials. The various carbon-based materials have received much attention as

a promising alternative to Pt. The many research groups have reported high photovoltaic performance with various carbon materials such as graphite, active carbon, carbon nanotubes.[11,16,17] The conducting polymers were also efficient counter electrodes in various redox electrolyte.[18-20] In these days, the other new approach of applying new inorganic materials such as metal carbide, metal sulfide, and metal nitride in counter electrode were shown good photovoltaic performance.[21-23] A popular topic of these studies is finding the inexpensive materials which had high conductivity or high surface areas.[9]

Moreover, transparent conducting oxide (TCO) glass which used as a substrate of counter electrode also has a drawback of cost originating from an expensive fabrication process. The TCO glasses commonly used in electrode are In-doped SnO_2 (ITO) or F-doped SnO_2 (FTO). Since TCO substrate is responsible for more than 40 % of the total device cost,[24] the DSSC using TCO-free counter electrodes are greatly interested in the viewpoint of low production cost. To obtain efficient cost device, the DSSCs using Pt and TCO-free counter electrode have been attempted in several groups. The DSSCs applied sub-micrometer sized graphite counter electrode18 achieved 6 % cell efficiency[25] and the metal carbide film with conductive carbon presented 6.6 % efficiency.[26] Park[27] and Sung group[28] utilized PEDOT and CSA doped PANI film used as a TCO and Pt-free counter electrode of DSSC, respectively, and demonstrated comparable photovoltaic performance compare to platinized TCO counter electrode. The active material coated on metal foil such as Ti foil or stainless steel is one of the most widely investigated TCO-free electrodes owing to its outstanding cheap cost, superior conductivity and facile synthesis.[29-

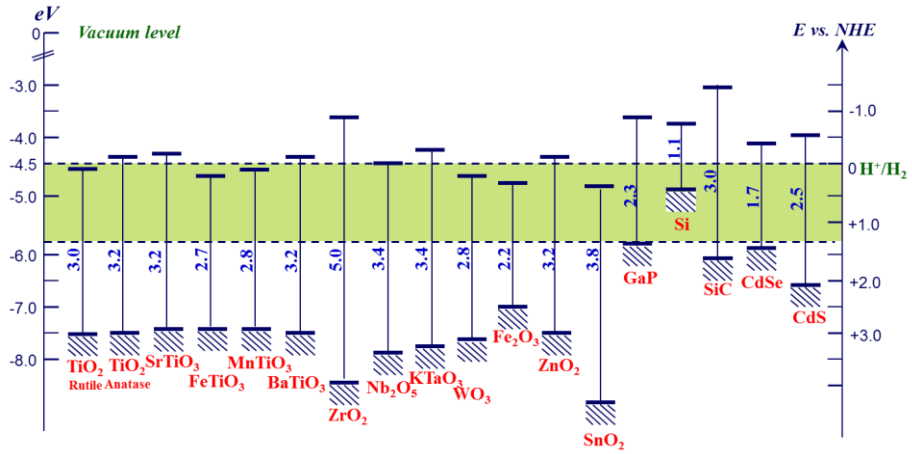

Figure 1.2. Band positions of materials for solar cells in contact with aqueous electrolyte at pH 0.[1]

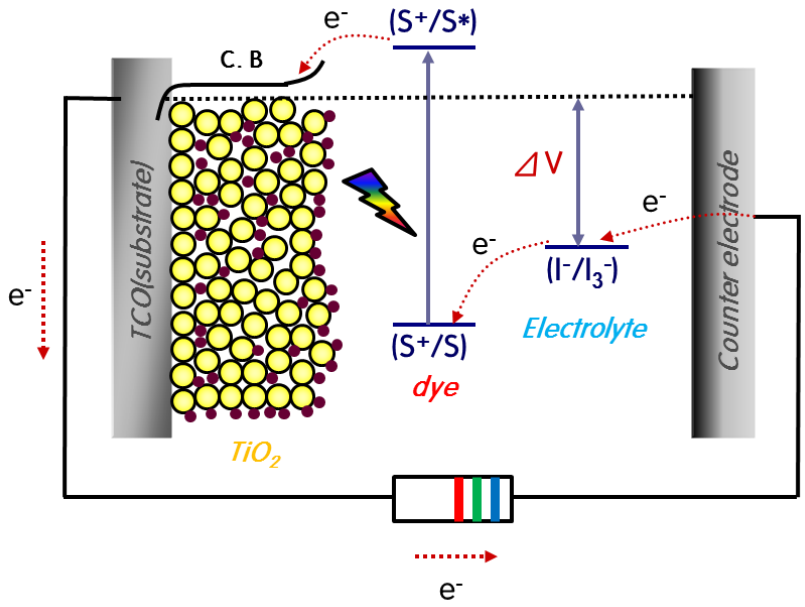

Figure 1.3. The schematic structure and operating principle of DSSCs.[13]

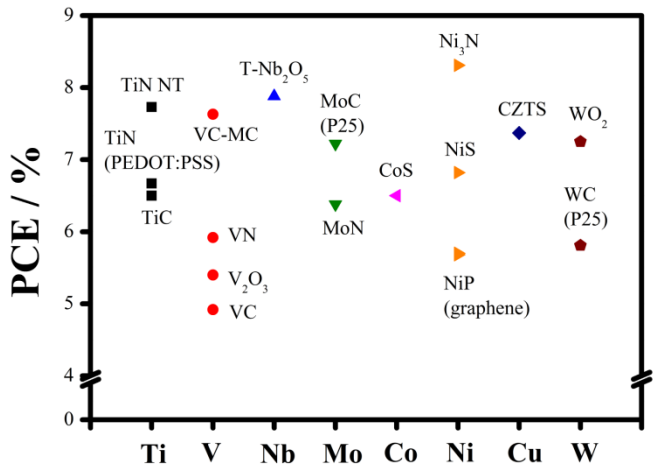

Figure 1.4. The distribution graph showing the conversion efficiencies of DSSC with alternative counter electrode.[15]

1.3 DSSCs analysis

Since DSSC is a photovoltaic cell which converts incident light to electrical energy, the photocurrent-voltage curve of the cell at the certain illumination could characterize the photovoltaic performance of DSSC. Effective generation of electrical power in solar cell is achieved by the capability of the photovoltaic device to produce voltage over an external load and current through the load at the same time. Because DSSCs is an electrochemical cell which is completely different from the classical solid-state junction photovoltaics, electrochemical analysis is useful to characterize the components of DSSCs. In particular, the electrochemical analysis in counter electrode is very powerful analysis tools because the iodide reduction reactions are occurred at the surface of it. In this study, the several electrochemical tests such as polarization test, electrochemical impedance spectroscopy, and cyclic voltammetry are used to analyze the counter electrode of DSSCs.

1.3.1 Photovoltaic cell performance

A photovoltaic cell is a device, which converts incident light to electrical energy. Generation of electrical power under illumination is achieved by the capability of the photovoltaic device to produce voltage over an external load and current through the load at the same time. This is characterized by the photocurrent-voltage curve of the cell like as Figure 1.5. When the cell is short circuited under illumination, the maximum current, the short circuit current (I_{sc}), is generated, while under open circuit conditions no current can flow and the voltage is at its maximum, called the open circuit voltage (V_{oc}). The point in the iv-curve yielding maximum product of current and voltage, maximum power, is used to define the fill factor which is important factor of solar cell performance.

$$\text{Fill factor (FF)} = \frac{V_{max} \times I_{max}}{V_{oc} \times I_{sc}} \quad (1.1)$$

The maximum power output of the solar cell can be calculated as fill factor and, the energy conversion efficiency of the solar cell is demonstrated as a power produced by the cell divided by the power incident on the representative area of the cell

$$\eta = \frac{V_{oc} \times I_{sc} \times FF}{P_{light}} \quad (1.2)$$

1.3.2 Electrochemical test

1.3.2.1 Polarization Test

Polarization test is general test for identifying the electrochemical properties. It can be conducted by current sweep or galvanostatic method. Because current sweep method is not steady-state measurement, EIS is necessary to compensate for steady-state result. The exchange current density (J_0) was a parameter which presented in the absence of net reactions and at zero overpotential. For calculating an exchange current density (J_0) on the surface of the electrodes which varies inversely with the charge transfer resistance (R_{ct}), and it could be estimated as below equation.[21,31]

$$J_0 = \frac{\mathrm{RT}}{\mathrm{nF}R_{ct}} \quad (1.3)$$

This exchange current density could be compared the slope of the Tafel plot such as Figure 1.6. If the slopes of the cathodic and anodic branches were small, it indicates that the lower electrocatalytic activity was presented. Furthermore, at a low sweep rate, the limiting diffusion current density (J_{lim}) depends on the diffusion coefficient (D) and Warburg impedance (W_s) of the redox couple in the

electrolyte as mentioned in literature.[21, 22, 31] If the large J_{lim} values was shown, which induces a relatively higher diffusion coefficient and low Warburg impedance as calculated from following equations.

$$D = \frac{l}{2nFc} j_{lim} \tag{1.4}$$

$$D = \left(\frac{RT}{n^2 F^2 c_o A W_s}\right)^2 \tag{1.5}$$

During polarization test, the concentration of triiodide species is much lower than that of iodide to calculate the diffusion coefficient of the triiodide species.

1.3.2.2. Cyclic Voltammetry

The cyclic voltammetry (CV) was measured in a three-electrode electrochemical cell to measure the electrocatalytic activity of film. The working electrode, a Pt counter electrode, an Ag/AgCl (sat. KCl) reference electrode and liquid electrolyte were commonly used for CV measurement. In this thesis, acetonitrile solution dissolved 10 mM LiI, 1 mM I_2 and 0.1 M $LiClO_4$ was used as an electrolyte to find out the electrocatalytic activity of triiodide reductions.

Usually, Pt electrode which is widely used as a counter electrode of DSSC is known to be an excellent catalyst for iodide adsorption and dissociation processes. The electrochemical reaction about iodide is followed;

$$3I^- - 2e^- \rightarrow I_3^- \tag{1.6}$$

$$I_3^- + 2e^- \rightarrow 3I^- \tag{1.7}$$

The first reaction is occurred by injection of electrons into photo-oxidized dye from iodide ions in

the electrolyte in negative peak, and the second one is reduced produced iodide ion pm the electrode in positive peak.[32,33]

1.3.2.3. Electrochemical Impedance Spectroscopy (EIS)

Applying DC plus AC voltage with a frequency to an electrochemical system can cause the current response with phase difference. The phase difference and amplitudes of AC voltage and current can be showed as complex resistance, impedance. EIS is an effective technique to extract each component in an electric circuit.[34] The Nyquist plots of the each symmetrical cell were fitted to the Randles circuit (Figure 1.7(a)), consisting of Rct in series with the Warburg impedance (W_s), both of which being in parallel with a double layer capacitance (C_m). A series resistance (R_s) was introduced to describe the ohmic resistance of the load and the conducting substrates.[21] The R_s is determined by the impedance at high frequency where the phase is zero. The semicircle at the middle frequency is assigned to the R_{ct} and the corresponding C_m of the Pt/electrolyte interface. The other semicircle at low frequency refers to the Nernst diffusion impedance of the redox couple in the electrolyte.[31] The DSSC contains three spatially separated interfaces formed by FTO/TiO2, TiO_2/electrolyte, and electrolyte/Pt-FTO. Electron transfer which is coupled to electronic and ionic transport is illustrated in EIS spectra. The Nyquist plots of DSSC were measured at forward bias and fitted by the model refer to the literature (Figure 1.7(b)).[10] The R_s denotes the resistance of the electrolyte and the TCO substrate. R_{ct} and R were the charge transfer resistance of the interfaces of the counter electrode/electrolyte and porous electrode/electrolyte, respectively. The finite Warburg impedance (W_s) related elements were influenced by the diffusion in electrode/electrolyte interface.[35]

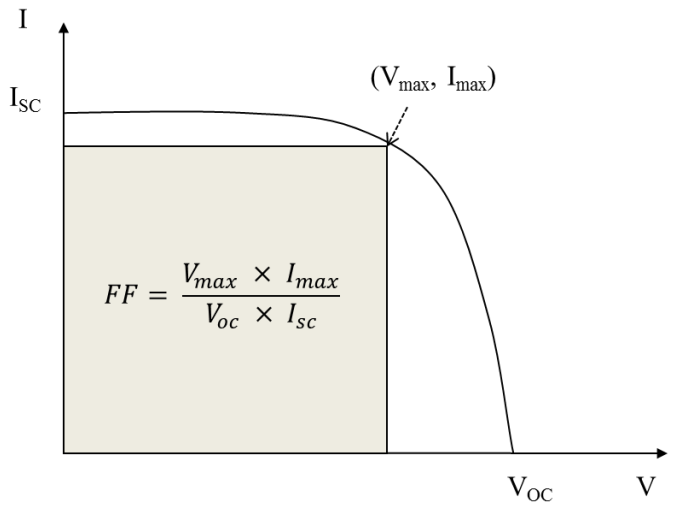

Figure 1.5. Characteristic of the solar cell performance in iv-curves.

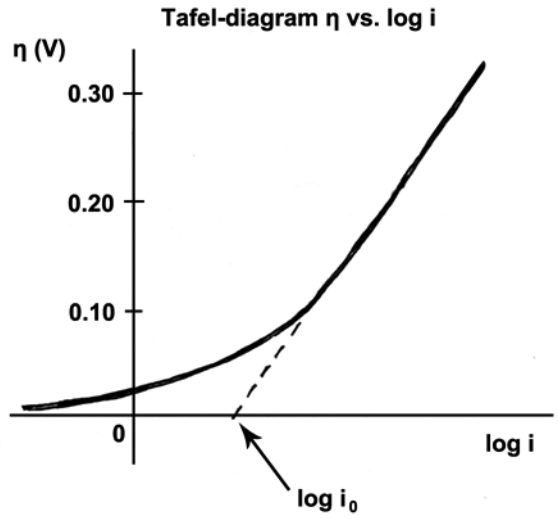

Figure 1.6. The calculating exchanging current from Tafel polarization curve.

(ref: http://en.wikipedia.org/wiki/File:100905_tafel_plot_nl.png)

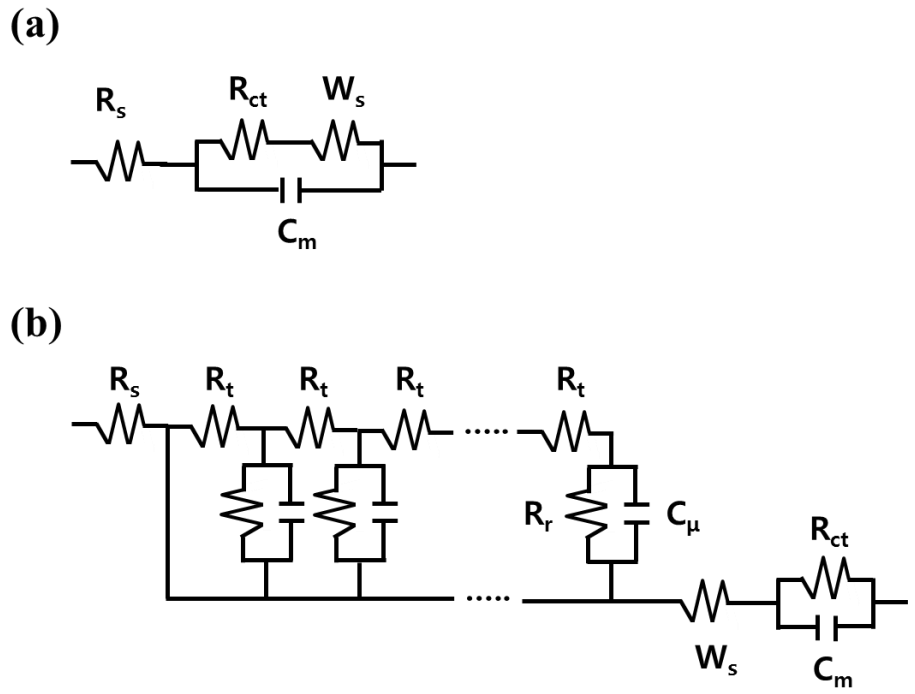

Figure 1.7. The equivalent circuits of (a) Randles circuit for dummy cells[21] and (b) DSSC devices.[10]

1.4 Subjects of this thesis

In this thesis, the main theme is application of Pt-free or Pt and TCO-free electrode as a counter electrode of DSSC and electrochemical analysis of these electrodes and DSSC devices. This thesis are consisted to two parts, Pt-free counter electrode and Pt and TCO-free counter electrode, as shown in Figure 1.8. And there are four different studies in them; (1) Pt-free counter electrode; poly(3,4-ethylenedioxythiophene) inverse opal electrode Ni nitride electrode film by sputtering at low temperature, and (2) Pt and TCO-free counter electrode; nitrided Ni metal foam electrode, camphorsulfonic acid-doped polyaniline electrode .

1.4.1 Pt-free counter electrode

Pt is a noble metal with very high cost, thus many efforts have been made to find alternative counter electrode materials to produce low-cost DSSCs. A lot of groups have researched replacing Pt counter electrodes with various conducting polymer materials, carboneous materials, metal nitride or carbide materials.

1.4.1.1. Poly(3,4-ethylenedioxythiophene) inverse opal electrode

The well-ordered porous structure of the inverse opal electrode provides some additional benefits as a DSSC electrode. First, the inverse opal electrode may have reduced mass transport limitations of the electrolyte due to its porous structure, and improves electrochemical reactions in various electrochemical devices.[36,37] These properties are resulted from the well-ordered porous structures

provide a large surface area for redox couple in the electrolyte. Second, the periodic nanostructures with long-range ordering also provide much easier electron transfer due to the better interconnections of the ordered structure.[38] In this study, we directly applied inverse opal structured poly(3,4-ethylenedioxythiophene) (PEDOT) electrode which was synthesized by PS opal template was a self-assembled electrode that was prepared in poly(3,4-ethylene dioxythiophene):poly(styrene sulfonate) (PEDOT:PSS) aqueous solution as a counter electrode without any extra processing in order to maintain the inverse opal structure.

1.4.1.2. Ni nitride electrode film by sputtering at low temperature

The transition metal nitrides in nitrided surface present the high electrocatalytic activity due to their noble metal-like electronic structures, and various transition metal nitrides such as MoN,[22] Ni_3N,[29] TiN,[24] W_2N,[31] were already reported as a highly efficient counter electrode for DSSCs. However, many researchers have shown that high temperature calcination using ammonia gas is necessary to obtain metal nitride, but it could be a barrier to get flexible counter electrode which used ITO/PET or ITO/PEN substrate. The R.F. sputtering method in present study was a low temperature deposition, and we could be obtained Ni nitride flexible electrode which was deposited on ITO/PET substrate. Furthermore, this Ni nitride film shown very thin thickness, this optically transparent Ni nitride flexible counter electrode was prepared on ITO/PET substrate successfully.

1.4.2 Pt and TCO-free counter electrode

This part was focused on the replacing expensive Pt and TCO into a conducting polymer. The

conventional platinized TCO glass counter electrodes are used as a catalyst layer and a charge transport layer, respectively. On the other hand, Pt and TCO-free counter electrode used in this paper functions two things in a single layer simultaneously, which is prepared using materials with high catalytic activity for I_3^- reduction and rapid charge transport ability.

1.4.2.1. Nitrided Ni metal foam electrode

Since the metal foam is three-dimensional porous metallic structure comprised of interconnected metallic particles with pores,[39] it can acts as a good electron carrier from the external circuit to the redox electrolyte compared to typically used substrate, TCO. In additions, open-pore structures in metal foam can be provided high surface areas to redox couple in electrolyte and reduced mass transport limitations of the electrolyte in electrode when it applied as an electrode of DSSCs. The transition metal nitrides electrode was a well-known high electrocatalytic materials because of their noble metal-like electronic structures.[29-31] Therefore, the nitrided Ni foam can be a new effective counter electrode without expensive Pt and TCO, which is novel method to fabricate cost-efficient counter electrode.

1.4.2.2. Camphorsulfonic acid-doped polyaniline electrode

The camphorsulfonic acid-doped polyaniline (PANI/CSA) film used in this thesis was shown high conductivity and excellent catalytic ability through simple spin-coating process. The PANI/CSA spin-coated on normal glass substrate by several optimization process, and it was successfully assembled as a counter electrode of DSSC. This film also can be operated by introducing light from both photoanode and counter electrode sides, which was called a bifacial DSSC, due to transparency

of the PANI/CSA film. Hence, it illustrated the promising potential for effective bifacial DSSC with Pt and TCO-free counter electrode by PANI/CSA film. Furthermore, we analyzed electrochemical properties of the PANI/CSA film coated on TCO-free glass substrate as a counter electrode and optical transmittance changes with electrochromism properties.

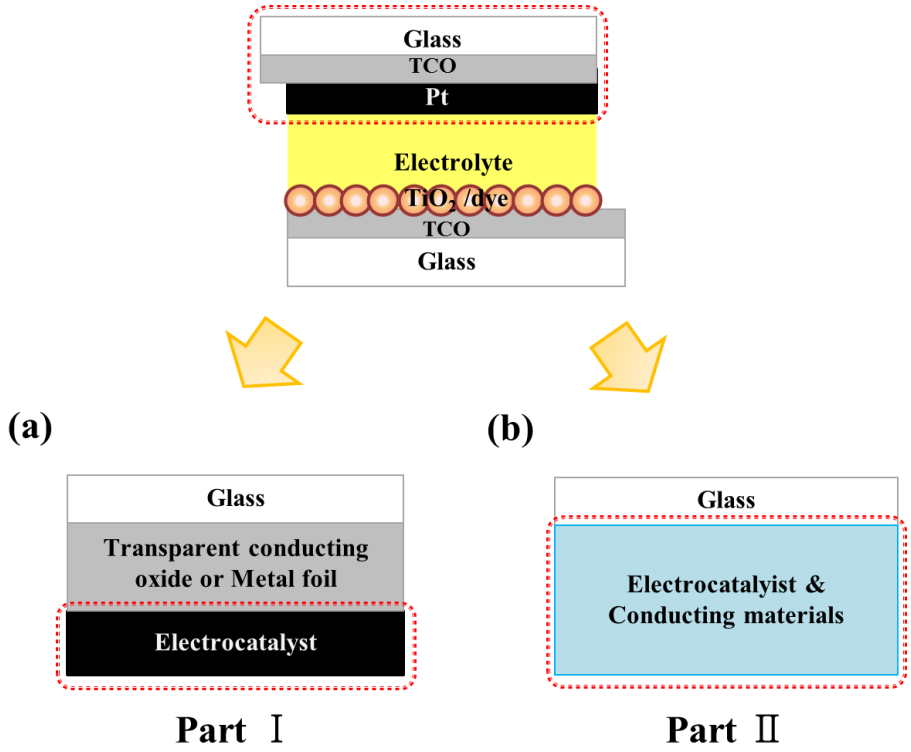

Figure 1.8. Schematic diagrams of the DSSCs for in this thesis; (a) counter electrode of DSSCs with the new electrocatalytic materials for Pt-free counter electrode and (b) counter electrode of DSSCs with Pt and TCO-free counter electrode.

Chapter 2. Experimental

2.1 Preparation of counter electrode

2.1.1 Poly (3,4-ethylenedioxythiophene) inverse opal electrode

The inverse opal structure was synthesized by etching an opal template from the film consisting infiltration materials within self-assembled opal template. 0.36 g of the 0.5 wt.% nonionic surfactant (Igepal® Co-30) and 80 mL of PEDOT:PSS dissolved aqueous solution (10 wt. %, Sigma Aldrich) were mixed together, and 0.5 g polystyrene (PS) suspension (Alfa aeser) was added. Nonionic surfactant was added to the PS colloid suspension to facilitate self-assembly and crystallization of the PS beads. Surfactant molecules were positively adsorbed on the surface, changing the hydrophilicity and surface tension properties of the suspension. The mixtures were then ultrasonicated for 30 min, and the FTO glass substrate was placed in an oven and dried for more than 2 days at 65 ℃ with constant relative humidity. PS particles were self-assembled into a structured crystal template during vertical deposition via water evaporation and sequential convective flux.[40] When the water was evaporated from the meniscus, particles constantly moved to the vicinity of the triple-phase contact line by convective fluid flow of the adjacent suspension. At the same time, capillary forces in the drying film pulled the spheres together to form an ordered close-packed structure. As a result, the film consisted of a PS opal structure with infiltrated PEDOT:PSS.

Cyclic voltammetry (CV) electrodeposition of PEDOT into the opal template was performed in a three-electrode cell using a Pt plate as counter electrode and an Ag/AgCl reference electrode using an

Autolab potentiostat (PGSTAT128N). The FTO substrate underneath the template served as the working electrode. Electrodeposition was carried out in a plating bath containing a solution of 0.05 M EDOT (3,4-ethylenedioxythiophene, Sigma Aldrich), 0.007 M sodium dodecyl sulfate and 0.1 M $LiClO_4$ (Sigma Aldrich) dissolved in distilled water. Based on a previous study[41], EDOT was polymerized using potential cycling between -0.3 V and 1.1 V vs. Ag/AgCl (0.3 M NaCl). The number of cycles was changed to control the thickness of PEDOT electrode. After the PEDOT was deposited, the film was immersed in toluene for 12 h at room temperature to dissolve the PS template and then dried in a 65 ℃ oven.

2.1.2 Ni nitride film deposited by sputtering at low temperature

The flexible Ni nitride films using in this paper were prepared on ITO coated glass or PET film. The R.F. magnetron sputtering (Korea Vacuum Tech) was used to prepare these films because this method was needed low temperature during film deposition. The substrate temperature was set to room temperature during each deposition. High purity Ni (99.99 %, RND Korea) metal was used as a target, and high purity Ar (99.99 %) and N_2 (99.99 %) were used as a reactive gas. The base pressure of deposition chamber was $5x10^{-6}$ mTorr. Pre-sputtering deposition under 10 mTorr Ar atmosphere was carried out for 12 hours to clean the targets and ensure steady state deposition. The Ni nitride deposition took place in two different gas, N_2 or Ar gas, with a total pressure was maintain 80 mTorr during deposition. During each film deposition, the reactive power and deposition time were fixed at 150 W for 3 hours as the optimized condition and the rigid ITO coated glass or PET films were used to obtain Ni nitride deposited electrode.

2.1.3 Nitrided Ni metal foam electrode

The Ni metal foam (500 μm) was purchased from the Metal Foam Korea and the Ni foil (125 μm) was also purchased from the Sigma Aldrich. The Ni foams were immersed in 0.1 M aqueous NaOH solution and dried in order to obtain to eliminate the impurities on foam surface. After cleaning process, the Ni foam was chemically etched with sulfuric acid (H_2SO_4) and nitric acid (HNO_3). Firstly, 10 wt % sulfuric acid and nitric acid was dissolved in distilled water and was controlled the temperature of solution, nitric acid treatment in RT and sulfuric acid treatment was 60 ℃. And then, the cleaned Ni metal foam was immersed in the prepared solutions for 20 mins and the solution was stirred using glass rod to remove the bubbels from the foam surface. This prepared Ni foams were nitrided in a box furnace at 450 ℃ for 2 h in ammonia atmosphere with a flow rate of 100 sccm. The nitrided Ni foams were thermally reduced in an 5 % H_2 atmosphere tubular furnace to reduce metal oxide part in nitride metal foams. Lastly, this prepared nitrided Ni foam electrode attached on a TCO-free glass substrate by surlyn (Dupont, 50 μm) to fix the Ni foam on glass.

2.1.4 Camphorsulfonic acid-doped polyaniline electrode

The aniline monomer purchased from Aldrich was used as received. Ammonium persulfate (APS) (98.0 %) and 10-camphorsulfonic acid (CSA) (98.0 %) were also obtained from Aldrich. Kokusan Chemical Co., Ltd (Tokyo, Japan) provided with m-cresol (98.0 %). Chloroform (CHCl3) (99.0 %), hydrochloric acid (HCl) (35.0~37.0 %) and ammonia solution (NH_4OH) (28.0~30.0 %)

were used as received from Samchun Chemical Co. (Seoul, Korea). Water and CHCl3 were mixed at a 1:2 volumetric ratio followed by the addition of HCl (96 mmol). The aniline monomer (22 mmol) was dropped into the solution followed by vigorous stirring. The APS solution was prepared by adding the APS powder (11 mmol) to the 5.76 M HCl solution (15 mL). At the desired reaction temperature, the APS solution was introduced into the monomer solution. The obtained PANI was washed and dried to give the green emeraldine salt form of the PANI powder. The as-prepared PANI was deprotonated with a NH_4OH 1 M aqueous solution. The dedoped PANI was rewashed followed by a drying step. For secondary doping, PANI and CSA were mixed at 2:1 molar ratio with a mortar and pestle. These mixture powders were dissolved in m-cresol with 3 wt%. The TCO-free glass substrate for deposition was cleaned successively in acetone, ethanol, and deionized (DI) water for 20 min in each step to remove any contaminations. Furthermore, in order to increase adhesion between PANI/CSA and substrate, a hydrophobic plasma treatment was conducted with CH_4 gas (200 W for 1 sec) at the ambient pressure. The PANI/CSA dissolved solution was spin-coated on a prepared glass substrate and dried at 50 ℃. After drying, the PANI/CSA coated glass was heated on a hot plate at various temperatures for 30 min to determine the thermal treatment effect.

2.2 Physical and electrochemical Analysis of electrode

2.2.1 Physical characterization of electrode

The thickness and morphology of the Ni nitride film were confirmed by field emission scanning electron microscopy (FE-SEM, SUPRA 55VP, Carl Zeiss) at an acceleration voltage of 2 kV. To determine the chemical composition of Ni nitride film, X-ray photoelectron spectrometer (XPS) was operated on surface of film and 300 sec etching using VG Scientifics (Al-Kα source). The results were calibrated by referencing C1s at 285 eV and fitted using Avantage software. The structure of electrode was estimated by X-ray diffraction (XRD) (Rigaku Corp., D-MAX2500-PC). Atomic force microscopy (AFM, XE-70, Park Systems, Korea) in tapping mode was used to examine the surface morphology of the films. Absorptions of films were observed by using a UV/Vis/NIR spectrometer (JASCO V-570) and transmittances of films were measured by using a UV/Vis spectrometer (Scinco, S-3100).

2.2.2 Electrochemical Analysis

Cyclic voltammetry (CV) was measured in acetonitrile solution dissolved in 10 mM LiI, 1 mM I_2 and 0.1 M $LiClO_4$ as an electrolyte at scan rate of 50 mV s^{-1} using potentiostat (Autolab PGSTAT30). The electrical impedance spectra (EIS) test and Tafel polarization test with symmetrical dummy cell were carried out to compare the electrocatalytic activity of Ni nitride film. The dummy cell was fabricated with two identical electrodes and concentration of triiodide in electrolyte is much lower than that of iodide (triiodide/iodide = 0.075 in molar ratio). Tafel-polarization curves were

measured with potentiostat at 50 mV s^{-1} scan rate and scan range from -0.6 V to +0.6 V. The electrical impedance spectra were measured at 0 V using an impedance analyzer (IM6, Zahner elecktrik) and a frequency ranging from 0.05 to 10^5 Hz with 10 mV of amplitude.

2.3 Photovoltaic performance and Analysis of DSSC

2.3.1 Electrode assembly for DSSCs

The μm-scaled TiO_2 films with an active area of 0.2 cm^2 were prepared by the deposition of a viscous TiO_2 paste (Ti-nanoxide D/SP, Solaronix) on F-doped SnO_2 (FTO) glass (8 Ω cm^{-2}, Pilkington TEC glassTM). N719 dye (Ru[LL0-(NCS)2], L=2,20-bipyridyl-4,40-dicarboxylic acid, L'=2,2'-bipyridyl-4,40-ditetrabutylammonium carboxylate, dyesol) was then adsorbed in the fabricated TiO_2 electrode as a sensitizer. The prepared TiO_2 electrode was assembled with a counter electrode into a sandwich-type cell using thermal adhesive films (Surlyn: 30 μm, Dupont). A drop of the redox electrolyte was injected into the cell.

2.3.2 Characterization of DSSCs

The photocurrent–voltage (I–V) characteristics of the assembled DSSCs were evaluated using a 500 W xenon lamp (XIL model 05A50KS source units) with a light intensity of 1 sun (100 mW cm^{-2}), which was adjusted using an NREL fabricated Si reference solar cell. The incident photon-to-current efficiency (IPCE, PV measurements,

Inc.) was measured from 300 nm to 800 nm under short circuit conditions to identify the quantum efficiency of each wavelength.

The electrical impedance spectra were measured at -0.7 V in darkness using an impedance analyzer (IM6, Zahner elecktrik) and a frequency ranging from 0.05 to 10^5 Hz with 10 mV of amplitude. The Nernst plot of EIS was plotted by using the equivalent circuit model which presented in the part of 1.2.2.3.

Chapter 3. Results and Discussion

3.1. Pt-free counter electrode for DSSC

3.1.1 Poly(3,4-ethylenedioxythiophene) Inverse Opal electrode

3.1.1.1 Preparation and morphology of PEDOT inverse opal electrode

As shown in Fig. 3.1(a) and (b), the PEDOT deposited in the PS opal template synthesized in the PEDOT:PSS aqueous solutions resulted in a more uniform surface with fewer defects compared to the one that was synthesized in pure water. It seems that the PEDOT:PSS conductive material, which was infiltrated with PS particles, provided several benefits for gradually filling the PEDOT into the opal structure from the substrate. Good interfacial contact between the electrode and the conducting substrate can give rise to good infiltration of PEDOT into the PS opal template. This fully infiltrated inverse opal structure provided efficient electron transport paths.[36,42] In addition, the change in the PS opal film surface by adding PEDOT:PSS in opal particles also had effected on electrodeposition. Because EDOT polymerization was performed in an aqueous solution to reduce template degradation in organic media[41], the hydrophilicity of template is an important factor for successful infiltration. The changes in the opal template surface were determined by static angle measurements with water. (Fig. 3.1(c) and (d)) The PS opal film synthesized in the PEDOT:PSS aqueous solution had an angle of 43±0.5°, which was smaller than that of the PS opal film synthesized in pure water (121±1°). The decrease in the contact angle resulted that the template with PEDOT:PSS infiltrated into PS opal particles has larger hydrophilicity.[43] Thus, it could be assumed

that the EDOT monomer in aqueous solution could easily penetrate into the PS opal template during electropolymerization, leading to the high quality infiltration of PEDOT into the PS opal template. Therefore, the self-assembled PS opal film synthesized in PEDOT:PSS aqueous solution was a superior template for an inverse opal electrode compared to that of commonly used PS opal film, which is synthesized in pure water.

The FE-SEM images in Fig. 3.2 show the comparison of the surface images between the conventional PEDOT (c-PEDOT) electrode and the inverse opal PEDOT (IO-PEDOT) electrode after removing the PS opal template, by the surface images. As shown in Fig. 3.2(a) and (b), the well-ordered 420-450 nm circle-shape pores and 40-50 nm thick PEDOT three-dimensional networks were exhibited in the IO-PEDOT electrode. Though the IO-PEDOT electrode presented spherical pores arranged in ordered arrays, the c-PEDOT electrode had aggregated PEDOT particles on the FTO glass (Fig. 3.2(c) and (d)). The spherical void sizes of the PS opal were smaller than the initial size of the PS particles in the IO-PEDOT electrode. Based on preliminary studies, many researchers have shown that high temperature calcination is necessary to remove the opal template to obtain a highly ordered inverse opal electrode. However, this method caused severe pore shrinkage, or destruction of the entire electrode structure.[44] The inverse opal electrode in present study was prepared by removing the opal template with toluene without any thermal treatment. Less than 10 % shrinkage of the air spheres was observed compared to that of the PS opal template.

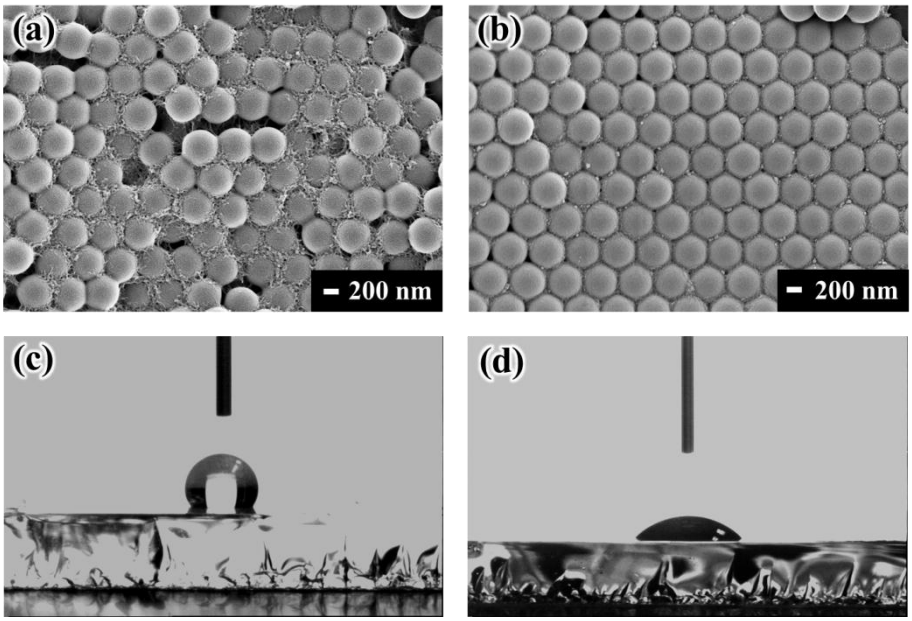

Figure 3.1. FE-SEM surface images and static angle images of different polystyrene (PS) opal templates; (a) and (c) are PS opal template with pure water, (b) and (d) are PS opal template with PEDOT:PSS aqueous solution.

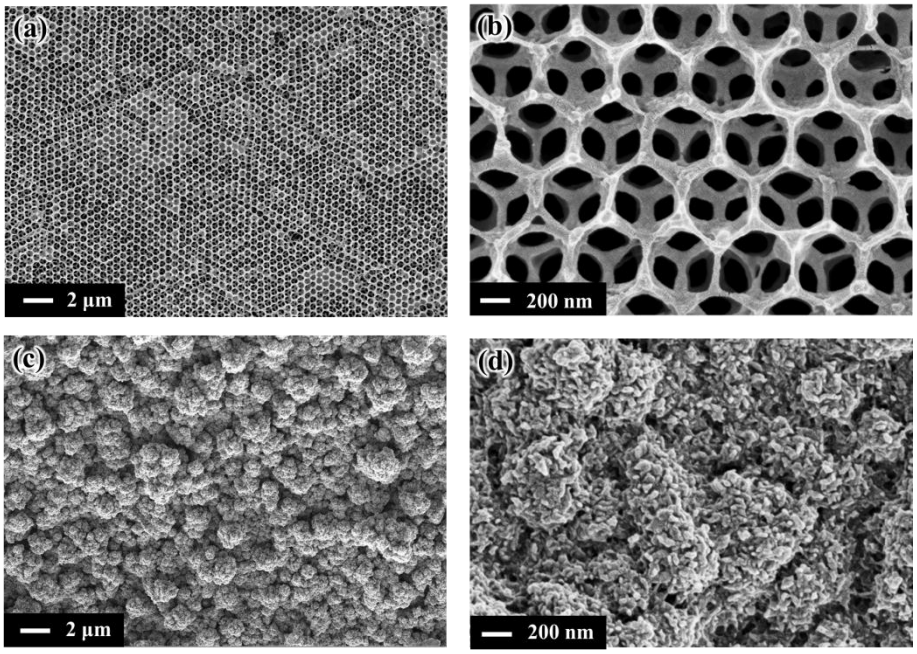

Figure 3.2. FE-SEM images of the surface morphologies of the IO-PEDOT electrode and c-PEDOT electrode; (a) and (b) are IO-PEDOT electrode, (b) and (d) are c-PEDOT electrode.

3.1.1.2 Electrocatalytic analysis of PEDOT inverse opal electrode

This electrode with ordered macroporous structures and air pores provided a high specific surface area and was regarded as a potential candidate as a counter electrode due to its high catalytic efficiency in electrochemical tests.[38]

CV was used to compare the electrocatalytic activity for triiodide reduction between the inverse IO-PEDOT electrode, c-PEDOT electrodes, and Pt electrode. According to the CV curves in Fig. 3.3(a)., the cathodic and anodic reactions for PEDOT or Pt deposited FTO electrodes were occurred reversely in iodide redox electrolyte. The inverse opal structured PEDOT electrode showed the highest cathodic peak current of −1.6 mA cm^{-2}, whereas the cathodic peak current of −1.1 mA cm^{-2} was observed for c-PEDOT and −0.9 mA cm^{-2} for Pt deposited FTO electrode. This result indicated that the IO-PEDOT electrode showed superior electrocatalytic activity for triiodide reduction even if it was a Pt-free electrode. The IO-PEDOT electrode also exhibited twice higher cathodic current density compared to those of a c-PEDOT electrode. This improvement in electrocatalytic activity by the IO-PEDOT electrode was due to the increased surface area induced by porous morphology shown in Fig. 3.2. The porous structure improved the electrocatalytic activity of the tri-iodide redox reaction in electrode.

The electrochemical impedance spectra (EIS) of the symmetrical cell, which was made with two identical electrodes, were assessed and compared the results from the literature to identify the electrocatalytic activity of the IO-PEDOT electrode. The Nyquist plots of each symmetrical cell are shown in Fig. 3.3(b) and analysed by Randle circuit model.[21] As shown in Table 1, which lists the

fitted results using Z-view software, the R_s values of the c-PEDOT and IO-PEDOT electrodes were 7.3 and 6.9 Ω cm^2, respectively. They were both lower than the R_s value of a Pt electrode (7.7 Ω cm^2). This could be due to either the high electrical conductivity between the PEDOT films (c-PEDOT or IO-PEDOT) and the FTO substrate compared to Pt electrode.[31] The IO-PEDOT electrode on the FTO substrate had the lowest R_s value among the electrodes depicted in Nyquist plots, demonstrating that the collection of electrons from the external circuit was promoted by the three-dimensional network structure of the IO-PEDOT electrode. Moreover, the R_{ct} values which refers to the electrocatalytic activity of the film were 2.02 Ω cm^2 for the c-PEDOT electrode, 0.16 Ω cm^2 for the IO-PEDOT electrode, and 0.21 Ω cm^2 for the Pt electrode. The R_{ct} of the IO-PEDOT electrode was 10-times better than compared to that of the c-PEDOT electrode, which was even lower than the R_{ct} value of Pt electrode. This indicates that the inverse opal structures of a IO-PEDOT electrode can show improved catalytic activity in reduction of triiodide to iodide, with effectiveness as high as that of Pt.[22,31] The largest Cm value was observed in the IO-PEDOT electrodes compared to that of the c-PEDOT electrode or Pt electrode. It additionally indicated that larger surface area was provided by the IO-PEDOT electrode due to the inverse opal structure.[30] In addition, a large Warburg diffusion resistance (W_s) was observed in the IO-PEDOT electrode, because of the porous inverse opal structure and the thicker layer of the electrode.[31] Therefore, these results indicated that the IO-PEDOT electrode possesses large surface area for high catalytic activity but provided lower diffusion velocity of the redox couple electrolyte. This behaviour is also presented in plot of current transient measurements in cobalt complex electrolyte. Because the size of the cobalt redox complex

is larger than that of the iodide redox complex, which is commonly used,[10] the mass transport limitations of the electrodes are more clearly shown by this measurement. DSSCs with cobalt complexes showed lower short circuit current density in i-v curves (Fig. 3.4(a)). The cobalt redox electrolyte was synthesized according to the method reported in the previous literature.[45] As shown in Fig. 3.4(b), the photocurrent density of DSSCs with cobalt complexes electrolyte decayed over a few seconds to lower steady-state though large initial current density generated immediately following illumination.[46] Compared to c-PEDOT or Pt electrodes, the IO-PEDOT electrode was the best in sustaining the initial photocurrent density generated in the cell, possibly due to the limitation of the photocurrent by diffusion that was reduced in the IO-PEDOT electrode due to the porous morphology of the inverse opal counter electrode.[12]

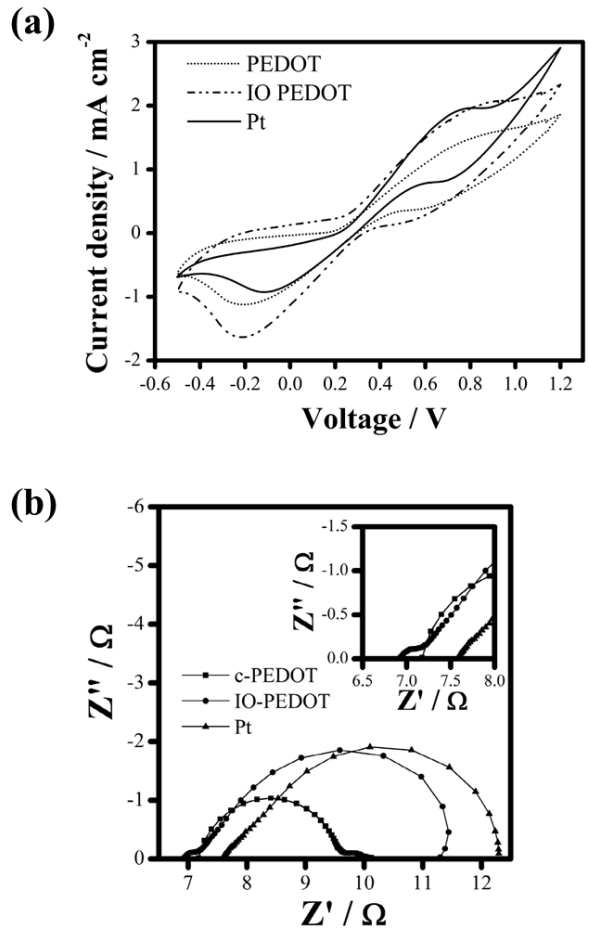

Figure 3.3. (a) Comparison of redox performances of PEDOT-based electrodes and the Pt electrode in iodide redox electrolyte by CV curves at 50 mV s^{-1}, (b) Nyquist plot of electrical impedance spectroscopy (EIS) curves of symmetrical cells of the c-PEDOT, IO-PEDOT, and Pt electrode.

Table 1. Parameters determined by fitting the electrical impedance spectra (EIS) of dummy cells.

	R_s /Ω cm^2	R_{ct} /Ω cm^2	Cm / μC	W_s /Ω cm^2
c-PEDOT	7.3	2.02	3.73	0.82
IO-PEDOT	6.9	0.16	210	4.22
Pt	7.7	0.21	13.9	4.06

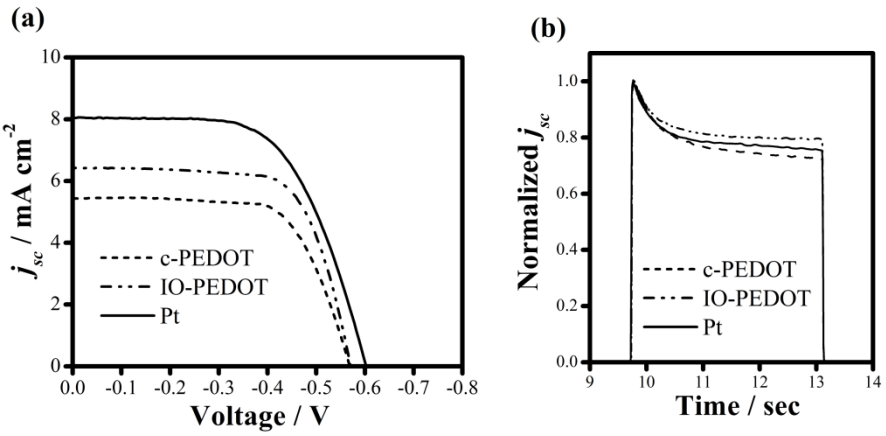

Figure 3.4. DSSC performances with c-PEDOT, IO-PEDOT, and Pt counter electrodes; (a) photocurrent–voltage characteristics of the DSSCs in cobalt redox electrolyte, (b) plots of the short circuit current density versus time by current transient measurements in cobalt redox electrolyte.

3.1.1.3 Photovoltaic performance and analysis of DSSC with PEDOT inverse opal counter electrode

The inverse opal electrode can reflect light at specific wavelengths depending on the photonic lattice size of the PS opals.[36] However, differences in reflectance were not clearly observed because the intensity was poor due to the thick PEDOT films. Thus, the effects of reflectance in the inverse opal counter electrode was considered by incident photon to current conversion efficiency (IPCE) with the DSSCs with N719 sensitized TiO_2 solar cells and IO-PEDOT counter electrode employing the iodide redox couple as the electrolyte. The normalized IPCE spectrum depicted in Fig. 3.5(b) showed significantly improved quantum efficiency at 300-450 nm at DSSC with IO-PEDOT counter electrode. This phenomenon is originated from the unique properties of the inverse opal structure that improved reflection at particular wavelengths. Therefore, the IO-PEDOT electrode can be synthesized into a well-ordered inverse opal structure on a substrate. The series resistance and charge transfer resistance of DSSCs with IO-PEDOT counter electrodes were reduced compared to those of DSSCs with c-PEDOT or Pt counter electrode. It was demonstrated by EIS curves at -0.6 V under dark conditions (Fig. 3.5(c)). The Nyquist plot of EIS curves were fitted with Z-view software, and the parameters are listed in Table 2. The much lower charge transfer resistance (R_{ct}) at the counter electrode and electrolyte, and high frequency in the EIS, was observed in the DSSC with the IO-PEDOT counter electrode, in contrast to the DSSCs with other electrodes. The enormous decrease in diffusion resistance (W_s) values in the inverse opal electrode is the main factor that leads to a reduction in series resistance. Therefore, the morphology of the inverse opal electrode provided

easy electrolyte transfer and higher electrocatalytic activity due to its porous structure. The fill factor was described to the sum of three resistances and could be expressed as below.

$$R_{total} = R_s + R_{ct} + R_{diff}(I_3^-) \qquad (4)$$

Thus, the improvements in the fill factor (FF) are ascribed to the reduction in series resistance of DSSC device[47] and the short current density of DSSCs was particularly increased in the gel-type electrolyte and liquid electrolyte as shown in Fig. 3.6 and Table 3. It was noted that the inverse opal PEDOT electrode have large pores in electrode because the DSS with IO-PEDOT counter electrode shown much improved performance in gel-type electrolyte corresponding to a conventional Pt counter electrode.

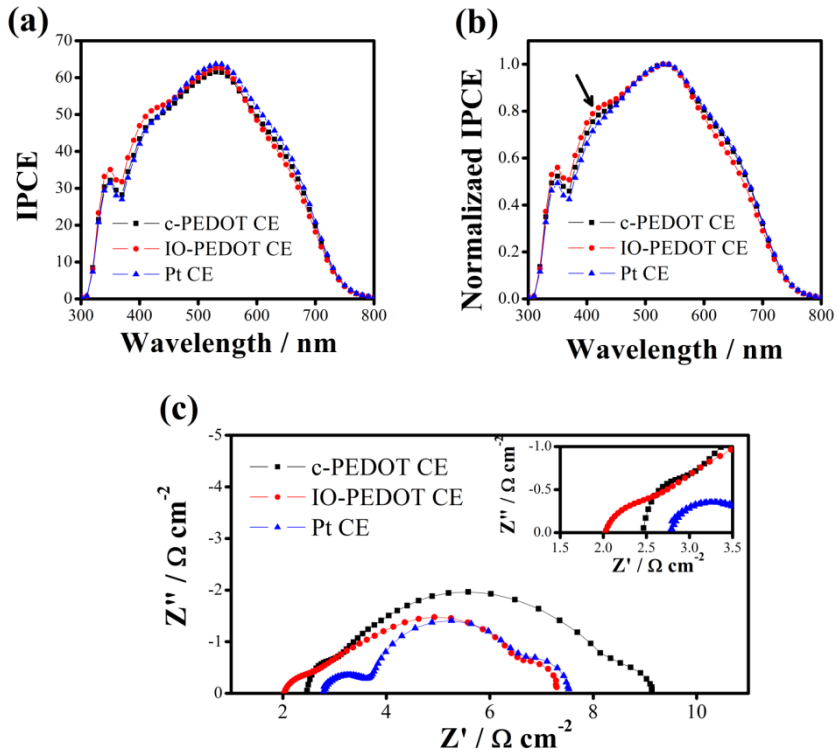

Figure 3.5. (a) IPCE of DSSC, (b) IPCE curves normalized to the maximum value, and (c) Nyquist plots of DSSCs from electrical impedance spectra (EIS) curves.

Table 2. Parameters determined by fitting the electrical impedance spectra (EIS) of dye sensitized solar cells (DSSCs) at dark conditions.

	R_s /Ω cm^2	R_{ct} /Ω cm^2	C_{ct} / μC	R_{TiO2} /Ω cm^2	W_s /Ω cm^2
c-PEDOT	2.5	0.49	110.6	18.5	5.1
IO-PEDOT	2.0	0.32	133.8	6.0	4.2
Pt	2.7	0.59	52.6	4.2	3.0

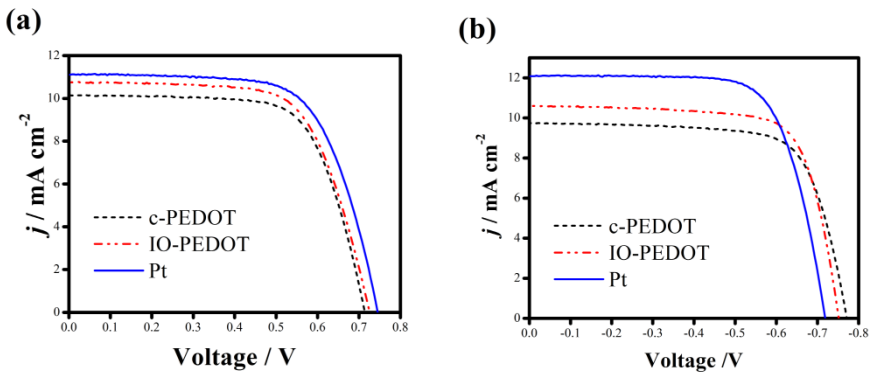

Figure 3.6. Photocurrent–voltage curves of the dye sensitized solar cells (DSSCs) with c-PEDOT, IO-PEDOT, Pt counter electrodes; (a) gel-type electrolyte, and (b) liquid-type electrolyte.

Table 3. Summary of the *j*–V characteristics of the dye sensitized solar cells (DSSCs) with c-PEDOT, IO-PEDOT, and Pt counter electrode.

		V_{oc} /V	j_{sc} /mA cm^{-2}	FF	η /%
gel-electrolyte	c-PEDOT	0.71	10.1	0.69	5.01
	IO-PEDOT	0.72	10.8	0.67	5.23
	Pt	0.71	11.05	0.61	4.85
liquid-electrolyte	c-PEDOT	0.77	9.74	0.72	5.43
	IO-PEDOT	0.75	10.59	0.74	5.87
	Pt	0.72	12.08	0.71	6.17

3.1.2 Ni nitride film deposited by sputtering at low temperature

3.1.2.1 Physical Characterization of Ni nitride film

Although metastable metal nitrides have complex phase diagrams, Ni–N system presents only a few phases well identified. By gradually increasing the nitrogen content, starting from pure Ni, the face-centered cubic (f.c.c) $(Ni_4N)_I$ and its face-centered tetragonal (f.c.t) modification $(Ni_4N)_{II}$ first appear, then the hexagonal cross- packed (h.c.p.) Ni_3N, and finally the body-centered tetragonal (b.c.t.) Ni_2N.[48] The nitrogen content in reactive sputtered Ni nitride film can be changed by substrate temperature during deposition such as Fig. 3.7.The peak of Ni(111) preferential orientation (PDF #00-004-0850) is obtained by sputtering the Ni target in pure Ar gas. The chemical inactiveness of Ni and nitrogen appeared in order to very small heat of adsorption. Thus, Ni nitrides were formed by N^{2+} ions were incorporated into the deposited Ni but surface nitrided Ni target was not deposited during R.F. sputtering in nitrogen gas. After the sputtering gas changed from Ar gas to N_2 gas, Ni peak was not observed and only phase of Ni_3N and Ni_2N phases only shown in the XRD patterns. The peaks at 40.9, and 66.8° 2θ, which can be assigned to Ni_2N phase,[49] were found at Ni nitride film deposited at RT. On the other hands, the Ni nitride film deposited at 220 ℃ presented the peaks at 44.2° 2θ, which was indexed as a Ni_3N(111) (PDF #00-089-7096). The different Ni nitride was formed by different substrate temperature can be thought with the change of Ni lattice constant of each Ni nitride film. While Ni lattice expands remarkably with the increase of nitrogen flow ratio at RT deposition, which does not increase with the nitrogen flow at 220 ℃ deposition as refer to the literature.[50] This can be explained that nitrogen incorporation into the lattice was easy when the film

deposited at RT substrate temperature. Therefore, Ni_2N which had high content of nitrogen in Ni nitride deposited the films deposited at RT.

However, the nitridation or oxidation actually occurred on the surface of the metallic Ni metal foil or foam as demonstrated in X-ray photoelectron spectrometer (XPS) spectra with Ar ion sputtering. The binding energy of oxidation Ni nitride state (856.3 eV) was gradually disappeared and the binding energy of Ni-Ni or N-Ni bonds (853.2 eV) was only remained in bulk Ni nitride films. It means that the oxidized nitrided Ni which presented in surface of film was disappeared, but the only metallic Ni or pure Ni nitrides were left in the bulk state.[29] This change was given in XPS spectrum of $Ni2p_{3/2}$ with Ar ion sputtering in Fig. 3.8.

The Ni nitride film could clearly be identified with a profile analysis of XPS spectra in Fig. 3.9. The N-Ni bond in N1s XPS spectrum (Fig. 3.9(a)) was observed at 397.1 or 397.6 eV for the nitrided Ni, on the other hand, the peak at around 400 eV which mentioned binding energy of N_2 on the surface appeared in the all Ni films whether it was nitrided or not.[29] It means that nitrogen atoms penetrate into the lattice of metallic Ni and the prepared Ni nitride in the case of R.F. sputtering under nitrogen atmosphere. XPS spectrum of Ni2p, Fig. 3.9(b), was strongly different from those of the Ni nitride films sputtering the Ni target in pure N_2 gas (N_{RT}, N_{220}) and Ni film electrode sputtering the Ni target in pure Ar gas (Ni). First, the Ni film deposited under pure Ar atmosphere can be find out with $Ni2p_{3/2}$ peak of 855.1 eV which is assigned to characteristic of Ni^{2+} in Ni oxide (NiO).[29] Because the metallic Ni is reactive enough with oxygen so that the Ni surface was slowly oxidized if it was exposed at air, the XPS peak of NiO state was detected in the pure metallic Ni film. However, the

oxidation actually occurs on the surface of the metallic Ni, which is demonstrated in the analysis in XPS spectra with Ar ion sputtering. As shown in Fig. 3.8., the binding energy is 853.5 eV of metallic $Ni2p_{3/2}$ peak gradually appeared with 855.1 eV of NiO state with Ar ion sputtering. The Ni nitride film deposited at RT or 220 ℃ under pure N_2 atmosphere was illustrated similar XPS spectrum and observed two peaks at 853.2-853.3 eV and 856.3-856.2eV. The first peak of 853.2 eV could be attributed to $Ni2P_{3/2}$ for metallic Ni. The second one at 856.3 eV was higher than the binding energy of the characteristics of Ni^{2+} in NiO, and it confirms that part of Ni nitride has been oxidized to a high oxidation state such as Ni^{3+}. And the relative intensity ratio of the first to the second was about 2:1.[51] After all, it showed obvious Ni nitride synthesis by R.F. sputtering under nitrogen atmosphere as presented in binding energy of nitrogen and Ni elements in XPS spectrums. Furthermore, the relative atomic concentration of Ni and N obtained from XPS spectra was lower in Ni nitride film deposited at 220 ℃ compared to that of Ni nitride film deposited at RT.

Fig. 3.10(a)-(c) depict the FE-SEM surface images of Ni nitride films deposited at different temperatures RT and 220 ℃ and Ni thin film. The apparent surface differences were shown in Ni nitride films deposited at N_2 gas and Ni film deposited at Ar gas. It was considered that the metallic Ni and Ni nitride which was deposited at different gas were dissimilar lattice structure of Ni metal and Ni nitride. In additions, most of the Ni particles were homogeneously distributed on the thin film surface. The surface morphologies changes were shown in each Ni nitride film due to different shape and size of the Ni nitride grains. Since the surface of Ni nitride film deposited at RT was accumulated with square-shape particles and the size of particles about 20-30 nm, the Ni nitride film deposited

220 ℃ was presented more smooth surface which consisted to 15-20 nm spherical particles. This change of the morphology might be originated from the different substrate temperature owing to reducing grain boundary on high substrate temperature. The thin film deposited under nitrogen atmosphere was presented much thinner thickness compared to the thin film sputtered at Ar gas.[52] Since the thickness of metal Ni film was 70 nm, the Ni nitride thin films were depicted 20 or 30 nm thickness as presented in cross-section FE-SEM images (Fig. 3.10(d)-(f)). It was accounted that a slow sputtering rate in nitrogen gas nitrogen was functioning both as sputtering target and reactive gas as a formation of Ni nitride.

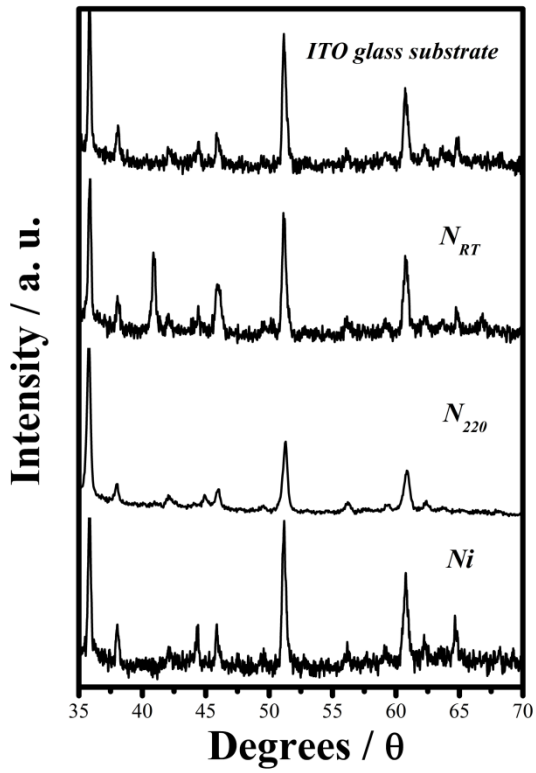

Figure 3.7. The XRD patterns of the Ni film deposited under Ar atmosphere and Ni nitride films deposited under N_2 atmosphere at RT (N_{RT}), 220(N_{220}).

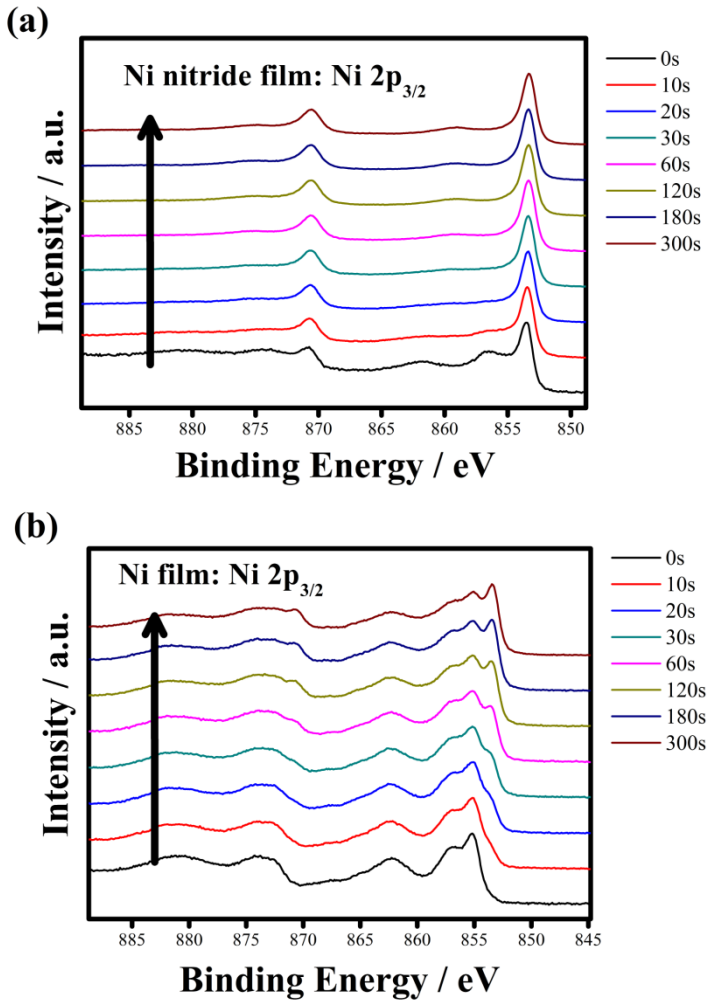

Figure 3.8. The Ni2p XPS depth profile of Ni film and Ni nitride film with Ar ion sputtering.

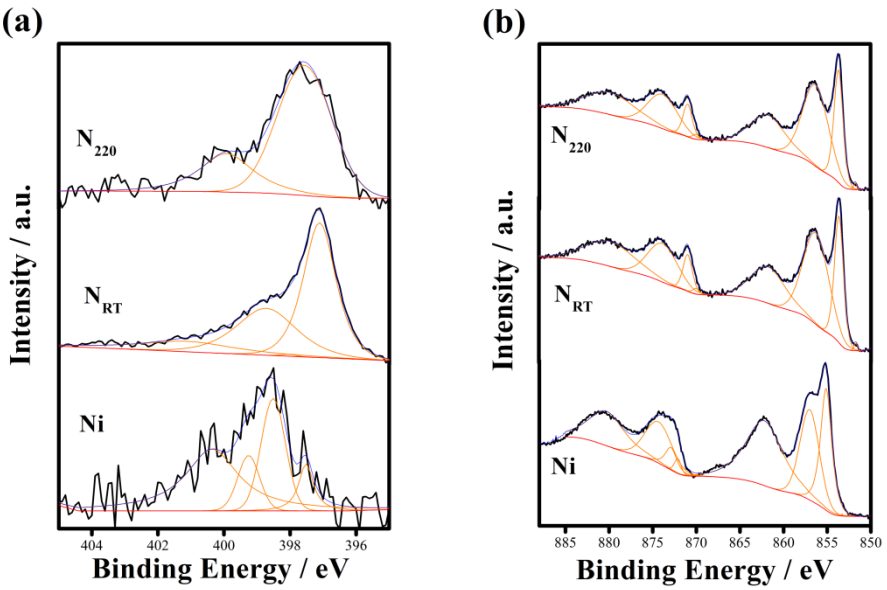

Figure 3.9. The comparison of N1s and Ni2p XPS spectrums of Ni film (Ni) and Ni nitride films (N_{RT}, N_{220}).

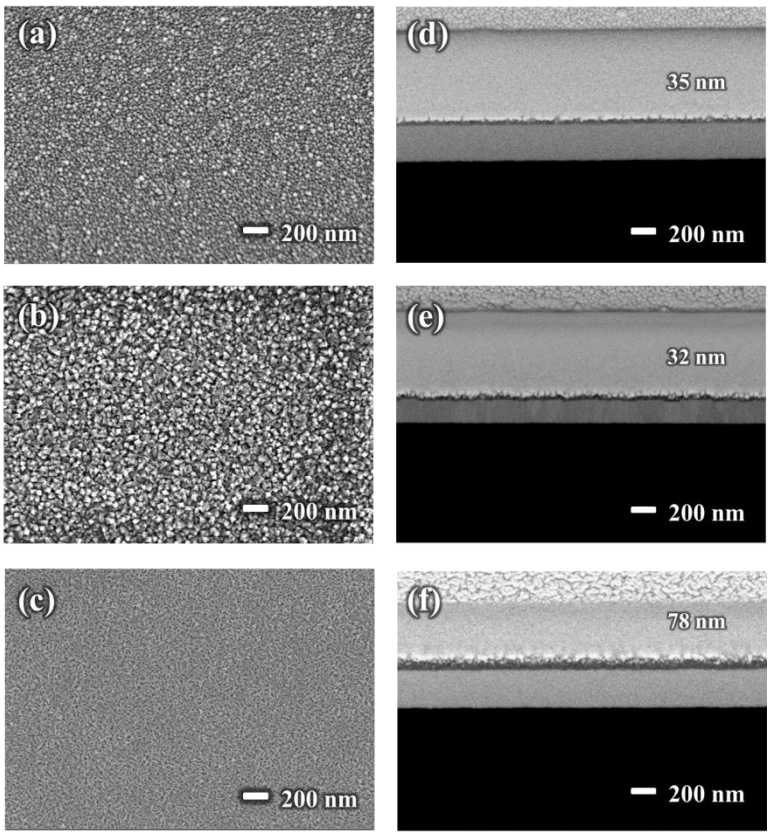

Figure 3.10. FE-SEM images of the films; the cross-sectional images of (a) N_{220}, (b) N_{RT}, and (c) Ni, and the surface images of (d) N_{220}, (e) N_{RT}, and (f) Ni.

3.1.2.2 Electrocatalytic analysis of Ni nitride film

A counter electrode should have electrocatalytic activity for triiodide reduction. Fig. 3.11(a) demonstrates the electrochemical impedance spectra (EIS) and Tafel polarization measurement of the symmetrical cell made by two identical electrodes were measured. Then, the results for dummy cells were fitted to the Randles circuit. As shown in Table 4 which listed the fitted results by Z-view software, the R_s values of the Ni nitride films sputtering in pure N_2 gas at RT (N_{RT}) and sputtering in pure N_2 gas at 220 (N_{220}) were 11.9 and 10.1 $\Omega\,cm^2$, respectively. They were both higher than the R_s value of the Pt electrode (9.6 $\Omega\,cm^2$). The resistivity increased after the introduction of nitrogen into the sputtering gas, and it could affect the higher electrical resistivity of metal nitride films compare to that of Pt metal film. This can be explained by impurity scattering effect because of the nitrogen concentration of Ni films.[48,53] On the other hand, the Ni nitride films were obtained different resistivity of films, and it seems to be caused by the difference of crystallinity, considering both XRD patterns shown in Fig. 3.7 and different morphology of surface shown in Fig. 3.10. Moreover, the R_{ct} values which refers to the electrocatalytic activity of film were 0.77 in N_{RT} film, 0.94 in N_{220} film, and 0.04 $\Omega\,cm^2$ in Pt electrode, respectively. The R_{ct} of N_{220} film was slightly improved compared to N_{RT} film, which is even much lower than the R_{ct} value of the Pt electrode. It illustrated that Ni nitride films can show the catalytic activity of reducing triiodide to iodide even if they were less effectively compare to Pt, and the N_{RT} film was estimated as a better counter electrode due to low charge transfer resistance. For comparison of C_m values, the largest C_m value was shown in N_{220} film compared to N_{220} film.

The Tafel-polarization measurements were also carried out in a symmetrical cell to confirm the electrochemical catalytic activity of Ni nitride electrodes.[21] Fig. 3.11(b) shows the logarithmic current density ($\log j_{sc}$) of each electrode as a function of the voltage. The slopes of the cathodic and anodic branches, which predicted an exchange current density (J_0), for the two Ni nitride films were smaller than that of the Pt film, and it indicates that the lower electrocatalytic activity was presented in Ni nitride films.[31] The slope of the Tafel plot in N_{RT} film was larger than that in N_{220} film, which is also in good agreement with the charge transfer resistance of EIS results which presented in Fig. 3.11(a). Furthermore, at a low sweep rate, the limiting diffusion current density (j_{lim}) depends on the diffusion coefficient (D) and Warburg impedance (W_s) of the redox couple in the electrolyte as mentioned in literature.[21, 31] The j_{lim} values of the N_{220} electrodes are larger than that of the N_{RT} electrode, which induces a relatively higher diffusion coefficient and low Warburg impedance.

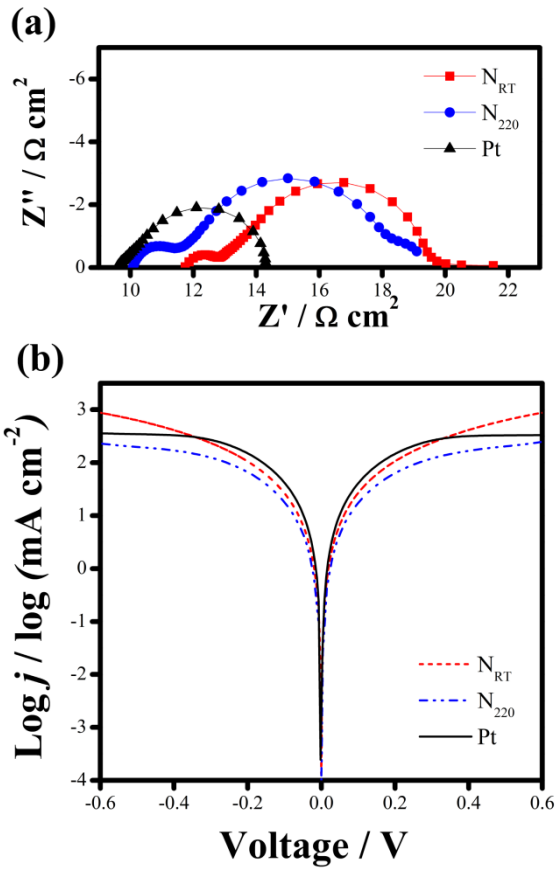

Figure 3.11. (a) Nyquist plot of electrical impedance spectroscopy (EIS) and (b) Tafel polarization curves of symmetrical cells of the N_{RT}, N_{220}, and Pt electrodes.

Table 4. Parameters determined by fitting the electrical impedance spectra (EIS) of dummy cells.

	R_s /Ω cm^2	R_{ct} /Ω cm^2	Cm / µC	W_s /Ω cm^2
N_{RT}	11.9	0.77	16.4	6.9
N_{220}	10.1	0.94	43.5	7.2
Pt	9.6	0.04	807	4.7

3.1.2.3 Photovoltaic performance of DSSC with Ni nitride counter electrode

Fig. 3.12 and Table 5 presented the performance of the Ni nitride counter electrodes in comparison to the Pt counter electrode using a conventional DSSC system which consisted of the photoanode, N719 dye-adsorbed 10 μm-thick anatase TiO_2 film on FTO substrate, and I_3^-/I^- redox couple electrolyte. To optimize the Ni nitride counter electrode conditions, the various deposition times were attempted as the key factor expected to be linked to the final efficiency. By increasing the deposition time from 3 hour to 10 hours, the thickness of film was increased from 32 nm to 102 nm and the amount of N-Ni bond on XPS spectrum was changed as presented Fig. 3.13 and Fig. 3.14, respectively. Therefore, the Ni nitride counter electrode deposited for 3 hours, which exhibited the best performance in the iodide electrolyte, was selected as the counter electrode of the DSSCs.

Although many researchers have shown that high temperature calcination using ammonia gas is necessary to obtain metal nitride, but it could be a barrier to get flexible counter electrode which used ITO/PET or ITO/PEN substrate.[29-31,54,55] However, the R.F. sputtering method in present study was a low temperature deposition, and we could be obtained Ni nitride flexible electrode which was deposited on ITO/PET substrate successfully and it was also applied to flexible counter electrode of DSSCs. The flexible Ni nitride electrode deposited on flexible In-doped in oxide (ITO) coated PET film was also shown the optical transparency. This flexible electrode was used as a counter electrode of DSSCs. The device consisted of the N719 dye-adsorbed 10 μm-thick anatase TiO_2 photoanode, gel-type iodide redox electrolyte and the Pt or Ni nitride flexible electrode. At 1 sun illumination, the performance of DSSC with the Ni nitride counter electrode deposited on ITO glass

was shown in the current-voltage curve of Fig. 3.12(a) and the IPCE spectrum of Fig. 3.12(b). While the DSSC with Pt counter electrode represented a short circuit current of 13.83 mA cm^{-2} and cell efficiency of 6.14 %, the DSSC with the N_{RT} counter electrode provided 13.26 mA cm^{-2} of j_{sc}, 5.51 % of cell efficiency and the DSSC with the N_{220} counter electrode provided 12.31 mA cm^{-2} of j_{sc}, 4.88 % of cell efficiency, respectively. In the current-voltage curve of DSSCs, the DSSC with Ni nitride counter electrode was shown lower fill factor and it was main reason for the lower efficiency. It could be considered to the higher resistance which illustrated in EIS curves of Fig. 3.15 and listed the fitting value by Z-view software in Table 6. Compared to DSSC with Pt counter electrode, the DSSC with Ni nitride counter electrode presented the increase in the R_s and R_{ct} at high frequency region. This incensement of resistances leaded to decrease of fill factor in DSSC device.

As shown in IPCE spectrum of Fig. 3.12(b), the higher quantum efficiency at low wavelength, from 350 nm to 500nm, was affected the higher jsc valued in DSSC with Pt counter electrode. Furthermore, the j_{sc} in DSSC with N_{RT} counter electrode was higher than that with Ni_{220} counter electrode. Even though the film was deposited on 220 ℃, series resistance (R_s) was not decreased. It demonstrated that the ITO/PET substrate did not get be damaged by heat, and the short circuit current (j_{sc}) of DSSC was not be limited by the series resistance and sheet resistance of device as below equation.[56]

$$j_{sc} = j_{ph} - j_0 \exp\left(\frac{q j_{sc} R_s}{nkT} - 1\right) - j_{sc}\frac{R_s}{R_{sh}} \quad (5)$$

The higher charge transfer resistance and series resistance of DSSC with N_{RT} counter electrode was shown in EIS analysis. This difference was originated from the different roughness with different deposition temperature, and the N_{RT} film which had rough surface was shown improved electrocatalytic activity in iodide redox electrolyte.

In order to the optical transparency of the Ni nitride deposited ITO/PET film, the DSSC with this counter electrode could absorb light from rear side illumination and could be used as a bifacial DSSC device. And the Ni nitride deposited ITO/PET film which showed high transmittance in the range of 450 nm to 600 nm could have an advantage of light absorption to dye from rear side illumination. The photovoltaic results under rear side illumination were also illustrated in Fig. 3.12(a) by dash lines and listed in Table 5.

Despite excluding the Pt materials in counter electrode, the DSSC with Ni nitride counter electrode which was deposited on ITO glass or ITO/PET film presented comparable conversion efficiency compared to conventional DSSC. This result means that the DSSCs with the flexible Ni nitride counter electrode which was deposited by R.F. sputtering method could perform promising cell efficiency compared to the device with conventional Pt counter electrode in iodide redox electrolyte.

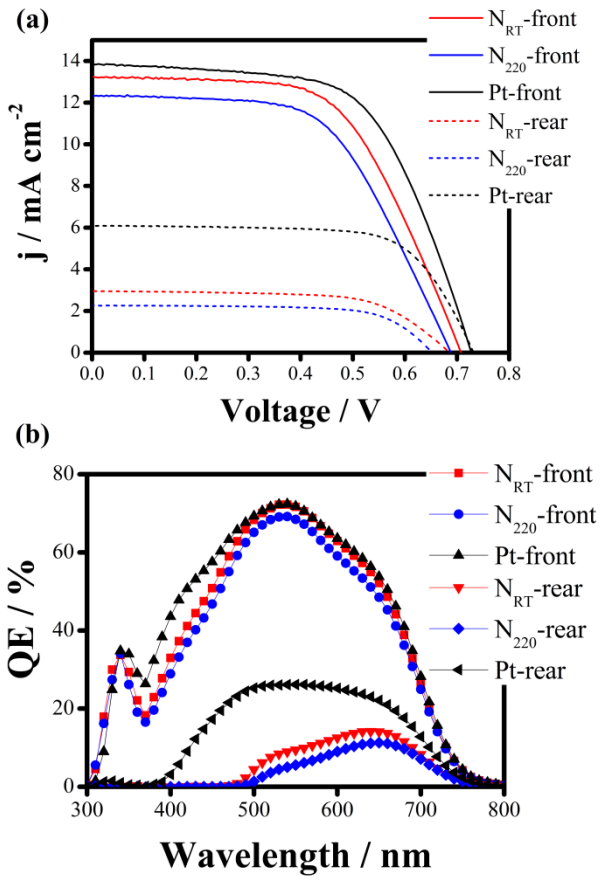

Figure 3.12. (a) current density–voltage characteristics of bifacial DSSC with Ni nitride (N_{RT}, N_{220}) and Pt counter electrode deposited on ITO/PET films, and (b) IPCE spectrums of these bifacial DSSCs with counter electrode deposited on ITO/PET films.

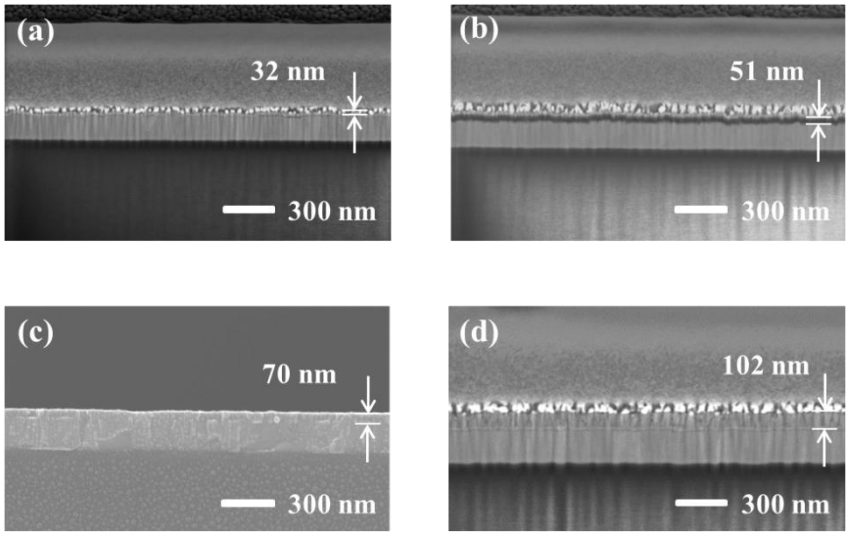

Figure 3.13. FE-SEM cross-sectional images of the Ni nitride films with various deposition times; the film deposited for (a) 3 hours, (b) 5 hours, (a) 7 hours, and (a) 10 hours.

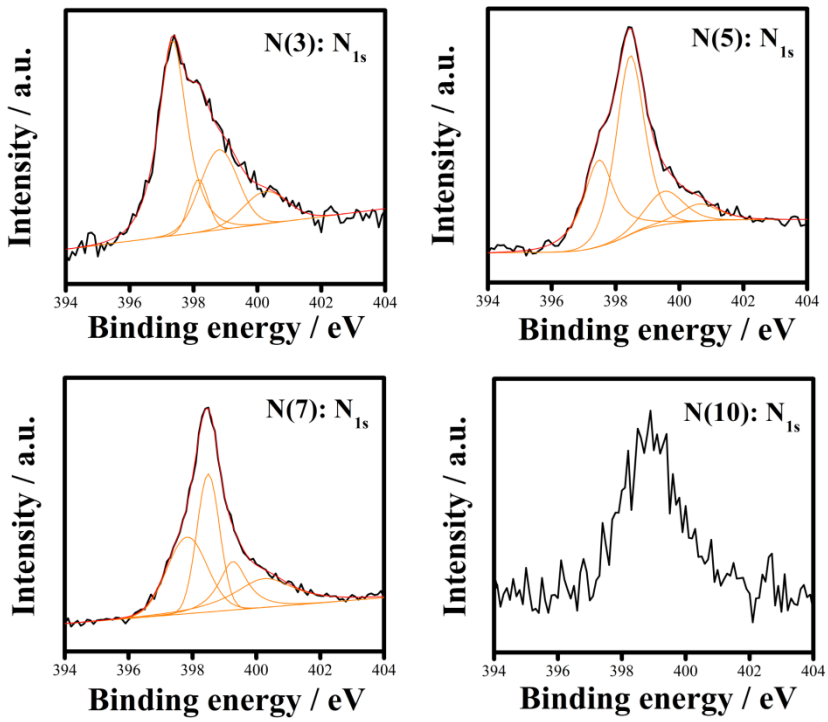

Figure 3.14. The difference in N1s XPS spectrum of Ni nitride films with various deposition times; N(3), N(5), N(7), N(10) were called the film deposited for 3,5,7,10 hours under nitrogen atmosphere, respectively.

Table 5. Summary of the *j*–V characteristics of the dye sensitized solar cells (DSSCs) with Ni nitride and Pt deposited on flexible ITO/PET film..

		V_{oc} /V	j_{sc} /mA cm^{-2}	FF	η /%
N_{RT}	front	0.70	13.26	0.59	5.51
	rear	0.68	2.82	0.65	1.25
N_{220}	front	0.69	12.31	0.57	4.88
	rear	0.65	2.27	0.69	1.02
Pt	front	0.72	13.83	0.61	6.14
	rear	0.72	6.10	0.69	3.08

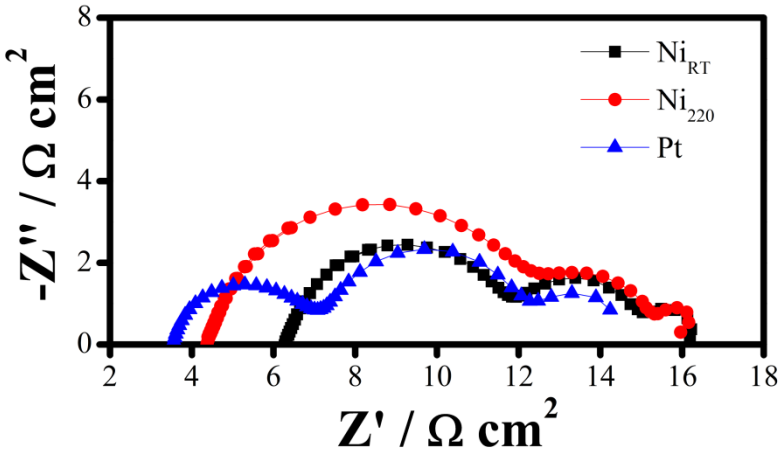

Figure 3.15. Nyquist plot of electrical impedance spectroscopy (EIS) of DSSCs with the flexible Ni nitride and Pt counter electrode at ocv condition.

Table 6. Parameters determined by fitting the electrical impedance spectra (EIS) of dye sensitized solar cells (DSSCs) at ocv conditions.

	R_s /Ω cm^2	R_{ct} /Ω cm^2	C_{ct} / μC	R_{TiO2} /Ω cm^2	W_s /Ω cm^2
N_{RT}	6.3	4.4	42.1	3.8	4.5
N_{220}	4.4	5.0	44.5	5.2	3.1
Pt	3.3	0.89	71.3	4.7	4.6

3.2. Pt and TCO-free counter electrode for DSSC

3.2.1 Nitrided Ni metal foam

3.2.1.1 Physical Characterization of nitrided Ni foam electrode

The comparison of FE-SEM images between nitrided Ni foam and foil was shown in Fig. 3.16. While the nitrided Ni foils have a relatively smooth surface, the Ni foam has a surface with the large pores dominated by three-dimensional structure. The thickness of nitrided Ni foil and foam were 117 and 458 μm, respectively. The Ni foam revealed the existence of interconnected structures that generate small and large open pores with compact and uniform surface.[57] In additions, the inside of interconnected structure was observed triangle-shape hollow space with 10 μm wall thickness was depicted in FE-SEM images of Fig. 3.17(a). The side of interconnected structure was consisted to small Ni grains as shown in the enlarge magnification FE-SEM surface images of Fig. 3.17(b). The porosity of porous structure of Ni foam was also demonstrated the measurement of density by Archimedean law, which calculated the density with water buoyancy, and compared it with density of Ni foil. Therefore, nitrided Ni foam presented density of 2.08 g cm^{-3}, it had porous structure which had 23.4 % relative density compared to theoretical density of Ni foil (8.83 g cm^{-3}) which was calculated by XRD (PDF#01-089-7128). Therefore, it was noted that the Ni foam had a very porous structure with 76.6 % porosity compared to Ni foil, and the mass transport in electrode might be improved due to this structure.[58-60]

The XRD patterns of Ni metal foil, Ni metal foam, and their nitrided ones are indicated in Fig. 3.18. All of the diffraction peaks of Ni foil and Ni foam after the nitridation can be apparently indexed to

the face-centered cubic (f.c.c.) Ni (PDF #00-004-0850). Although a preferential orientation of Ni (200) at 52 of 2θ is obtained in Ni foil or nitrided Ni foil, but a strong peak of 44 2θ was observed in Ni foam and nitrided Ni foam. The XRD patterns of Ni metal foams were different form that of Ni foils, but it was similar to that of Ni particles.[29] It noted that the Ni metal foam was comprised of interconnected metallic particles with well-oriented Ni particles to the (111) plane despite Ni plat foil shown the orientation at (200) plane. On the other hands, the very small peaks around 42, 52 of 2θ which corresponding to the peaks of NiO were detected in the nitridation treated sample. It was noted that the oxidation of metal foil or foam by air was also occurred during nitridation at 450 ℃ in ammonia atmosphere.

The nitridation or oxidation which was occurred in the metallic Ni metal foil or foam was analyzed by X-ray photoelectron spectrometer (XPS) spectra with Ar ion sputtering as demonstrated in Fig. 3.19(a). The binding energy of the oxidized Ni state, NiO, at 855.0 or 854.3 eV was observed on the surface, but they gradually disappeared with increasing Ar ion sputtering time. On the other hands, the binding energy of the pure Ni nitrides or metallic Ni was increased in the bulk state. Although the Ni oxide was shown in two electrodes, nitrided Ni foam and nitrided Ni foil, but the Ni nitride state was only observed in the surface of nitrided Ni foam. It was noted that the Ni foam was finely nitrided due to the porous structure and large surface area of Ni foam,[29] but the Ni foil was easily oxidized because metallic Ni surface was exposed in air because the dense Ni foil had non-nitrided surface.

While the binding energy of 853.6 eV, indicating a Ni nitride, was apparently observed in the bulk of nitrided Ni foam, but the binding energy of 852.3 eV, indicating a metallic Ni, and that of 853.8 eV for Ni nitride were appeared in the bulk of nitrided Ni foil. It was also illustrated that the relative nitrogen atomic concentration was dramatically decreased and the metallic Ni state was clearly increased in the all nitrided Ni electrodes with increasing Ar ion sputtering time. The electrical resistance of film which played a significant role in performance of electrode could be also affected by the bulk state. The resistance of nitrided Ni foam electrode was 3.3 $m\Omega\,cm^2$, and it was slightly larger than that of Ni metal plate (2.9 $m\Omega\,cm^2$). It might be due to the Ni nitride was observed in the Ni foam although the metallic Ni was shown in the Ni foil in the bulk state. However, these resistances were very similar to metal plate which was not nitrided and did not be a barrier to application as an electrode. Therefore, the metallic Ni in the bulk state could provide good electron transfer ability to surface-nitrided Ni foam, and it was an promising alternative substrate of TCO substrate.

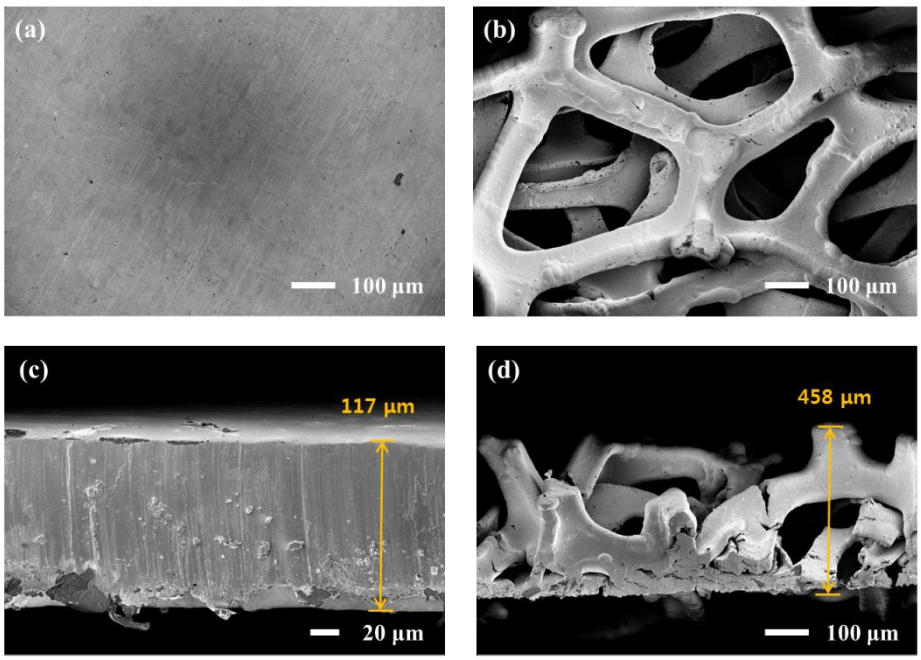

Figure 3.16. The comparison of FE-SEM images; the cross-section image (a) and the surface image (b) of nitrided Ni foam, the cross-section image (c) and the surface image (d) of nitrided Ni foil.

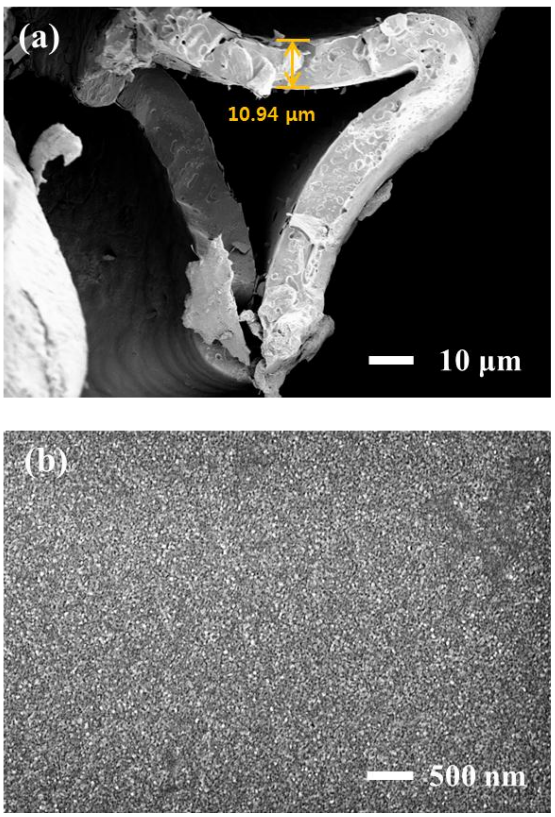

Figure 3.17. (a) The enlarged cross-section image of nitrided Ni foam and (b) the enlarged surface image of nitrided Ni foam.

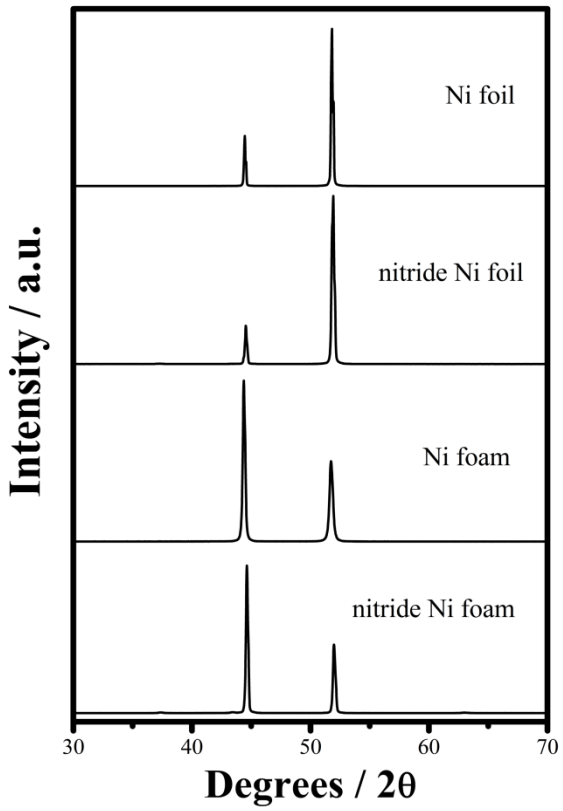

Figure 3.18. The comparison of XRD patterns of Ni foil, nitrided Ni foil, Ni foam and nitrided Ni foam..

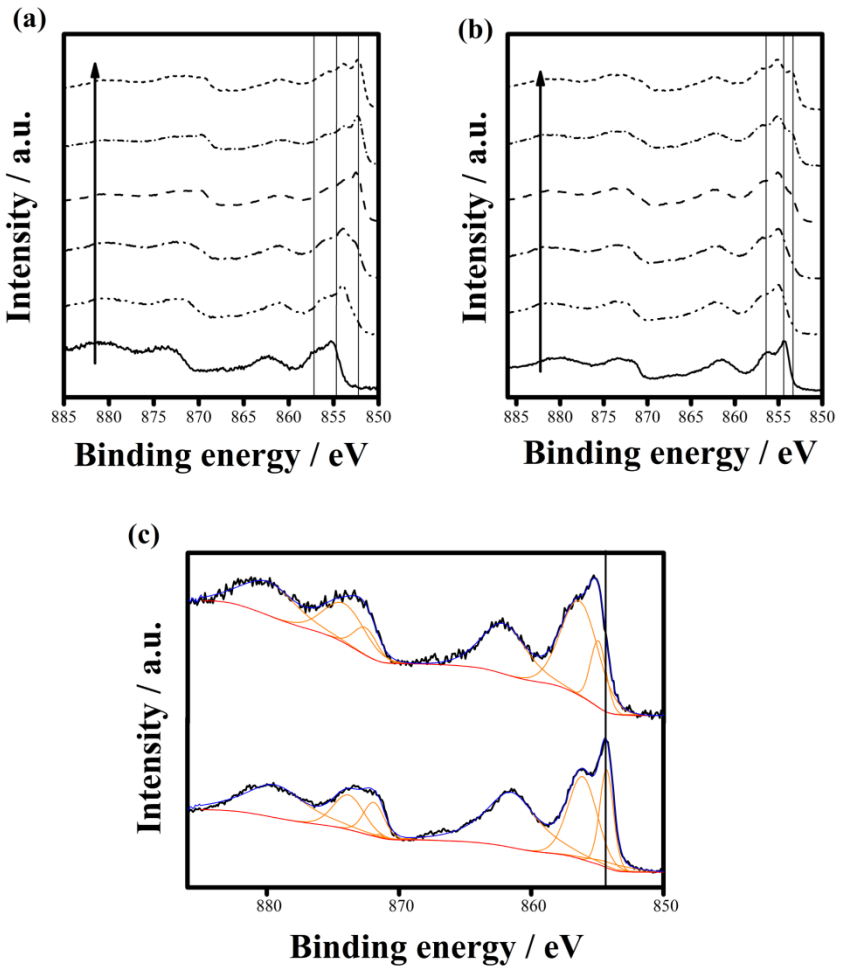

Figure 3.19. Ni2p XPS depth profile of nitrided Ni foil and nitrided Ni foam with Ar ion sputtering; (a) Ni2p XPS depth profile of nitrided Ni foil, (b) Ni2p XPS depth profile of nitrided Ni foam, and (c) comparison of Ni2p XPS spectrum of nitrided Ni foil and foam at the surface.

3.2.1.2 Incensement of surface area by chemical etching

The increased surface area induced by porous morphology could influenced the electrocatalytic activity of the tri-iodide redox reaction.[61-63] The nitrided Ni foams were prepared by chemical etching with two kinds of acid, nitric acid (HNO_3) and sulfuric acid (H_2SO_4), to increase the surface roughness of Ni foams.[57,61] The comparison of roughness between nitrided Ni foam, Ni(foam), and roughened nitrided Ni foam using sulfuric acid, Ni(H_2SO_4), and nitric acid, Ni(HNO_3) was depicted in atomic force microscope (AFM) images of Fig. 3.20(a)-(c). The root mean square (RMS) roughness of Ni(foam), Ni(H_2SO_4), Ni(HNO_3) were 20.1, 13.9, and 45.7 nm, respectively. It could be considered that the increment in roughness was attributed to chemical etching process, and this rougher surface could provide a larger surface area to increase iodide reduction in electrode. As shown in Fig. 3.21, the XRD patterns of Ni foams were not changed whether it was chemically etched with acids, but the wall thicknesses of nitrided Ni foams were slightly decreased with chemical etching by acid.

The comparison of electrocatalytic activity for triiodide reduction was demonstrated in CV curves for I^-/I_3^- redox about the nitrided Ni foams and Pt coated ITO glass. According to the CV curves in Fig. 3.22(a), different from the electrochemical behavior of Pt electrode, which exhibited cathodic peak and anodic peak, the nitrided Ni foam electrodes exhibited only cathodic peaks.[64] The acid treatment in Ni foam had greatly influenced on electrochemical activity of iodide reduction. The reduction peak current density of the Ni(HNO_3) (-2.52 mA cm^{-2}) and Ni(H_2SO_4) (-2.45 mA cm^{-2}) were significantly higher than that of Ni foam (-1.6 mA cm^{-2}). Furthermore, Fig. 3.22(b) indicates a

linear relationship between the scan rate and cathodic peak current. The adsorption of iodide species was slightly affected by the redox reaction on the electrode surface, but the major rate-determine step of the reaction was diffusion process.[32,65] In addition, the slope of the nitrided Ni foams which was attributed to the faster redox reaction[65] was changed with acid treatment, and the Ni(HNO_3) electrode was shown the largest slope among them. It can be ascertained that nitric acid treated nitrided Ni foam shown most superior electrocatalytic activity for triiodide reduction. In additions, the nitrided Ni foam used in this research demonstrated good reversibility and stability in the iodide redox couple because the nitrided Ni layer on the surface functioned as a protective layer of metallic Ni foam.[67] As can be seen in Fig. 3.23(a), the cathodic current density changed slightly after 100 CV cycles from −0.8 V to +0.5 V (vs. Ag/AgCl (sat. KCl)). Iodine typically reacts with the metal in the case of corrosion which causes then depletion of iodine in the electrolyte.[32] Because the loss of iodine by metal corrosion changes the color of the electrolyte from yellow to transparent color,[67-70] it could be found out the color changes of electrolyte. However, the electrolyte which used in CV cycling measurement was maintained yellow color, and the absorbance was also not changed color after the 100 CV cycling. The peak at 360 nm, which contributed to the iodide anion, was only observed in UV-Vis absorbance spectrum of Fig. 3.23(b). This result suggests that the nitrided Ni foams was not degraded by corrosion of metal substrate in iodide electrolyte, and it demonstrated good reversibility and stability in the iodide redox couple compared to platinized ITO film.

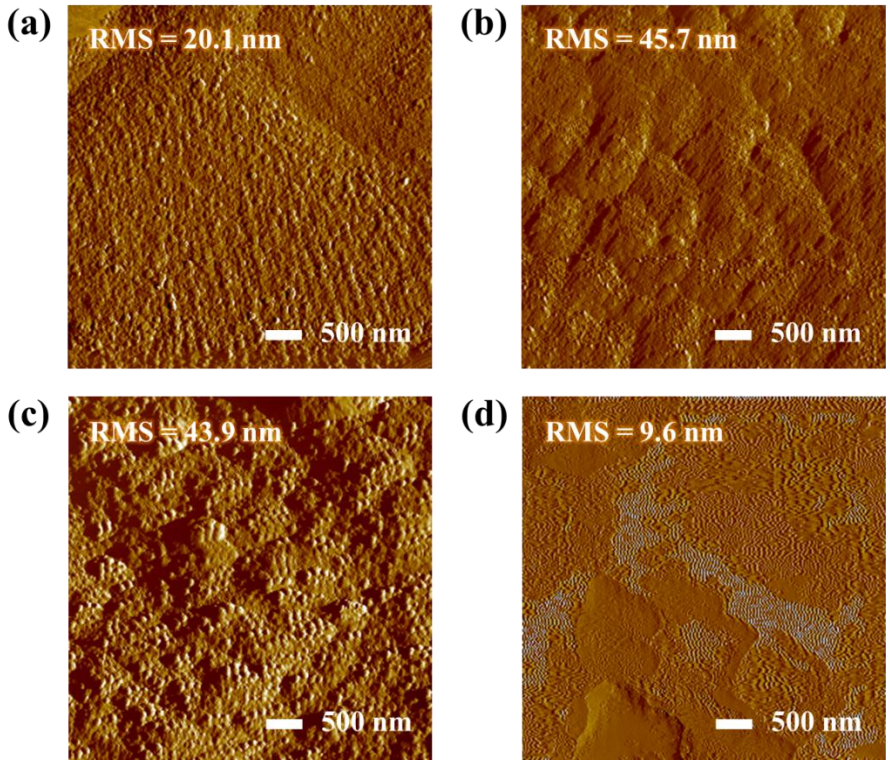

Figure 3.20. The comparison of AFM images of nitrided Ni foams and nitrided Ni foil; (a) Ni(foam), (b) Ni(H_2SO_4), (c) Ni(HNO_3), and (d) nitrided Ni foil.

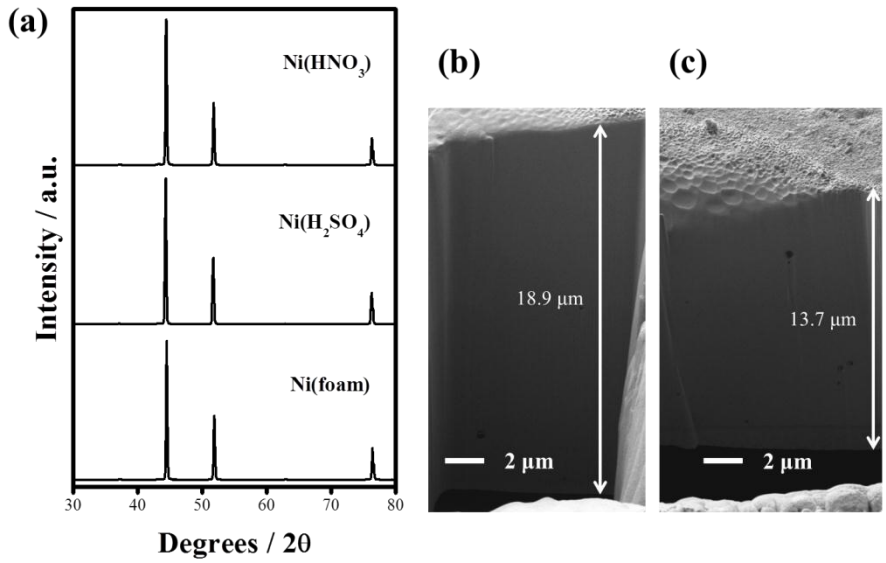

Figure 3.21. The comparison of XRD patterns and the thickness of nitrided Ni foams; (a) XRD patterns of Ni foams, (b) the cross-section images of Ni(foam), and (c) the cross-section images of Ni(HNO_3).

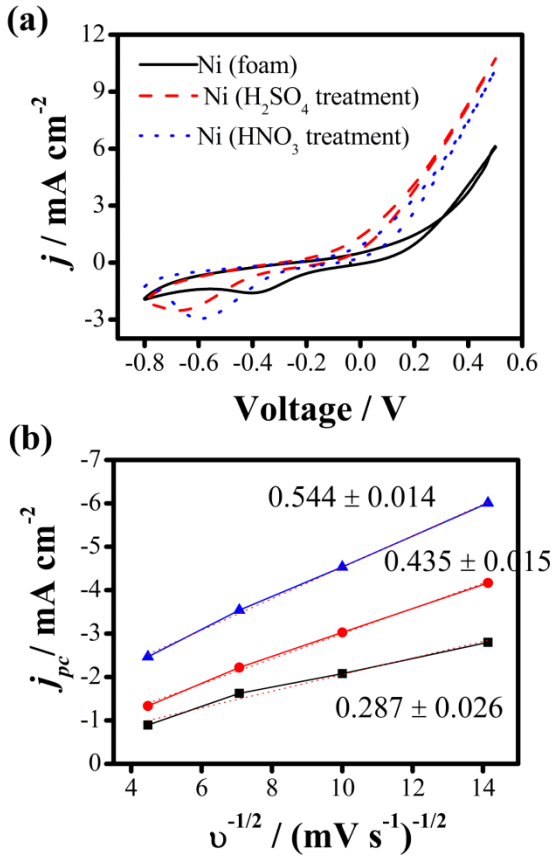

Figure 3.22. The comparison of redox performances of various nitrided Ni foams under iodide redox electrolyte; (a) CV curves at 50 mV s^{-1}, (b) relationship between (scan rate)$^{-1/2}$ ($v^{-1/2}$) and cathodic peak current density (j_{pc}).

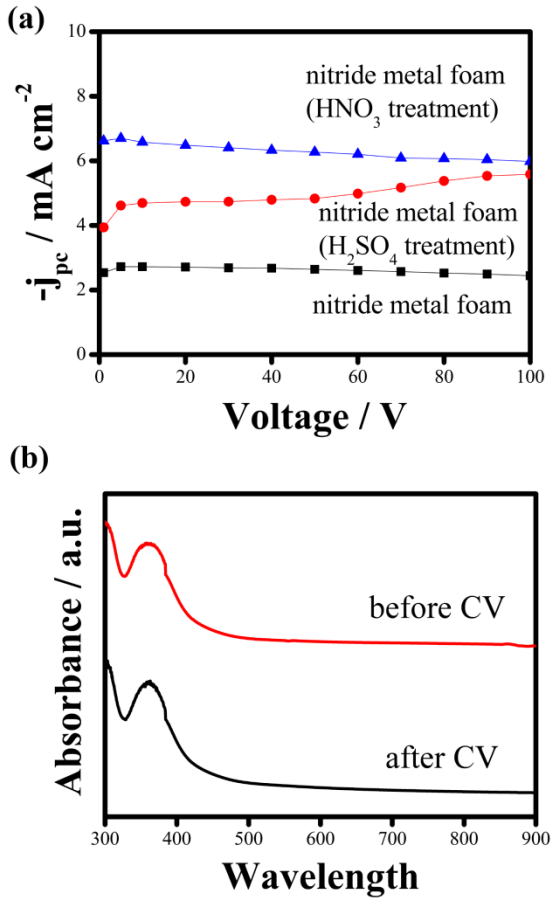

Figure 3.23. The stability of nitrided Ni foams in iodide redox electrolyte; (a) the changes in the cathodic peak current density (j_{pc}) during 100 CV cycles, (b) the comparisons of UV-Vis spectrums of electrolyte before and after CV measurement.

3.2.1.3 DSSC performance using nitrided Ni foam counter electrode

Fig. 3.24 demonstrated the comparison of DSSC performances using the counter electrodes with Pt coated ITO glass, nitrided Ni foil and different nitrided Ni foams. Table 2 listed performance of DSSCs with these counter electrodes. The conventional DSSC system which consisted of the photoanode, N719 dye-adsorbed 10 μm-thick anatase TiO_2 film on FTO substrate, and gel-type iodide redox couple was used at 1 sun front illumination condition. First of all, the nitrided Ni foil as the counter electrode was given poor conversion efficiency of 1.20 % due to poor electrocatalytic activity for reduction of triiodide. This low conversion efficiency and fill factor can be attributed to the nonporous texture and low active surface area. However, when the nitrided Ni foam electrode which had a porous morphology with interconnected structure of Ni grains was used as counter electrode, the photovoltaic performance had obviously enhanced because of a high active surface area.[29] The short circuit current density (j_{sc}) of DSSCs was particularly changed from 3.2 mA cm^{-2} to 9.6 mA cm^{-2}, and the FF was increased from 0.59 to 0.62. The nitrided Ni foam counter electrodes exhibited higher catalytic activity in EIS curves, Fig. 3.24(c), compared to nitrided Ni foil counter electrode. The lower charge transfer resistance (R_{ct}) at the counter electrode and electrolyte, which presented at high frequency in EIS, was observed in the DSSC with nitrided Ni foam counter electrode. The diffusion resistance (W_s) values decreased in nitrided Ni foam counter electrode due to the porous structures. It was noted that the higher catalytic activity and easy electrolyte diffusion were exhibited when Ni foam electrode was used as a counter electrode of DSSC. In addition, mass transport limitations of the electrolyte were affected because the nitrided Ni foam or foil was thick film. As

shown in current transient test (Fig. 3.24(b)), While the nitrided Ni foil was presented this tendency due to thick thickness, the nitrided Ni foam electrode could be sustained the initial photocurrent density generated in the cell because the limitation of the photocurrent by diffusion was reduced due to the porous morphology of Ni foam.[46] The diffusion resistance (W_s) values decreased apparently in nitrided Ni foam counter electrode due to the porous structures.

The chemical etching of Ni foam counter electrode was attempted to improve DSSC performance as illustrated in Fig. 3.25 and Table 7. First of all, the short circuit current density of DSSCs was particularly increased from 9.6 mA cm^{-2} to 10.6 and 11.3 mA cm^{-2} with chemical etching of Ni foam electrode. It was attributed to the rough surface by chemical etching provided a large surface area to iodide redox couple in electrolyte. The decline in charge transfer resistance (R_{ct}) in EIS of Fig. 3.25(b) also presented the improvement of iodide reduction in order to rough surface with chemical etching. The sum of all resistances of DSSC with nitrided Ni foam was lower than that of DSSC with Pt coated FTO glass because of low resistance of metal foam electrode. And this low resistance was benefit to fill factor and cell conversion efficiency of DSSC device. In additions, the metal based substrate influenced the current density of DSSC. To obtain efficient light harvesting in DSSC device, the scattering layers was attempted in many groups.[71-73] The counter electrode substrate can act as a back reflector and thus metal substrate may also increase the light harvesting in DSSC due to high reflectance.[67,73] As shown in Fig. 3.25(d), the reflectance of the Ni metal foam was larger than Pt coated TCO electrode, and the reflectance was decreased by nitridation treatment due to

formation of Ni nitride on the Ni metal foam surface. After nitridation under ammonia atmosphere, the color of Ni foam and the %R spectra were changed by acid treatment. Above all, the two kinds of nitrided Ni foam, Ni(H_2SO_4) and Ni(HNO_3), were shown the different %R spectra. While the Ni(H_2SO_4) electrode presented maximum reflectance at 550 nm, the Ni(HNO_3) electrode was lowest reflectance at 500 nm. Because maximum absorption value of dye is 510 nm, the Ni(H_2SO_4) electrode which also acted as a back reflector has benefit to increase light harvesting in DSSC due to high reflectance at 500 nm. This tendency was also depicted in IPCE spectrums of Fig. 3.25(c).

Accordingly, it was noteworthy that this nitrided Ni foam etched with nitric acid could be the best functioned counter electrode for DSSCs. This device exhibited a j_{sc}, V_{oc}, fill factor and cell efficiency of 10.6 mA cm^{-2}, 0.70 V, 0.64 and 4.76 %, respectively. The reference cell, DSSC with the platinized ITO counter electrode, displayed cell efficiency of 5.77 % as represented in Fig. 3.25(a). Therefore, the nitrided Ni foam counter electrode presented comparable conversion efficiency compared to conventional DSSC despite of excluding g the Pt and TCO materials in counter electrode. Therefore, it can be considered that the nitrided Ni foam electrode was promising candidate for the Pt and TCO-free counter electrode of DSSC. Furthermore, the other nitride metal foam can be applied as a cost-effective Pt and TCO-free counter electrode for DSSC.

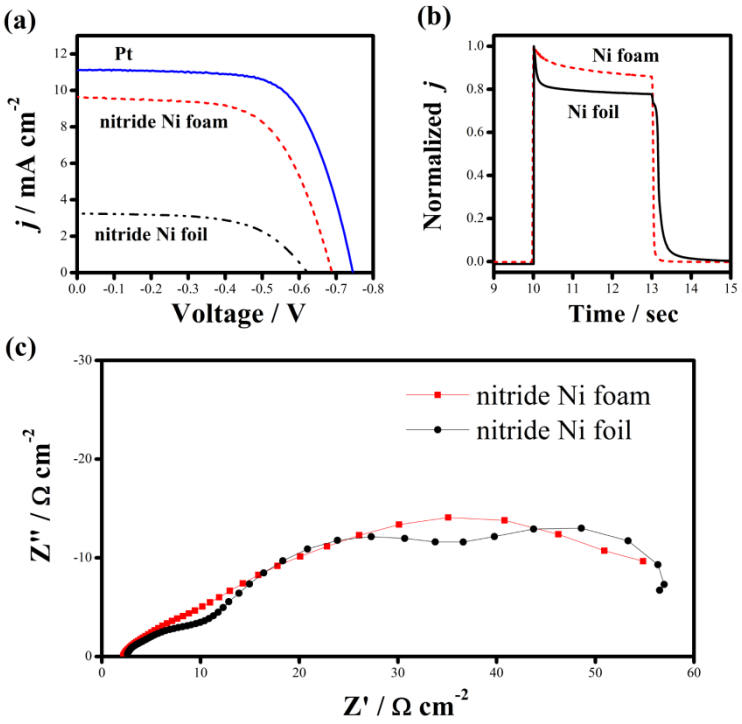

Figure 3.24. The comparison of the DSSC performance of the nitrided Ni foam and nitrided Ni foil counter electrode under iodide redox electrolyte; (a) current density–voltage curves of the DSSCs, (b) plots of the current transient measurement, and (c) Nyquist plots of the DSSCs from EIS curves.

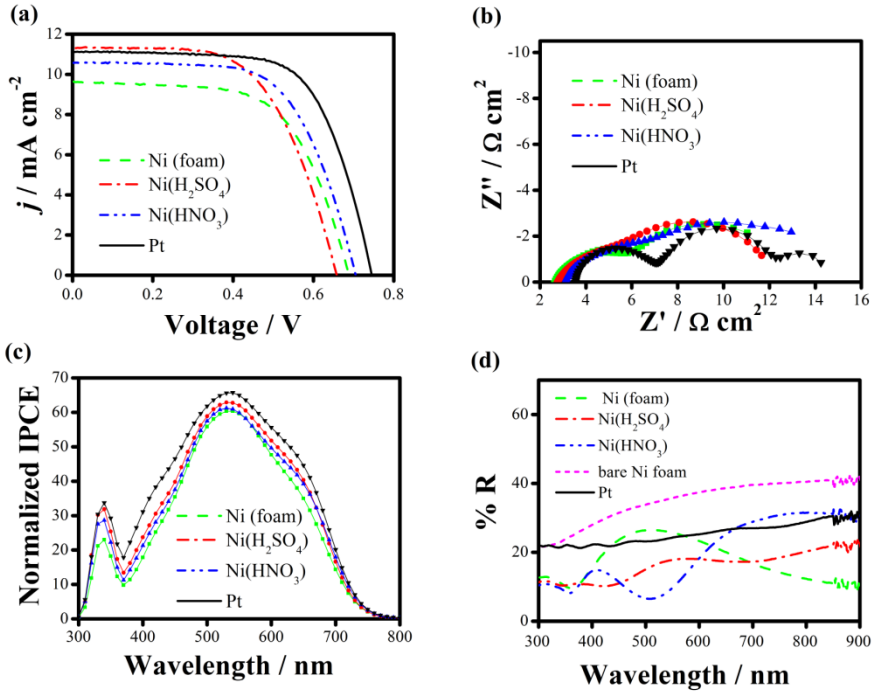

Figure 3.25. The comparison of the DSSC performance of the nitrided Ni foams with chemical etching, (a) current density–voltage curves of the DSSCs, (b) Nyquist plots of the DSSCs from EIS curves, (c) IPCE spectrum of the DSSCs, and (d) the %R spectra of nitrided Ni foams.

Table 7 Summary of the j–V characteristics of the dye sensitized solar cells (DSSCs) with various nitrided Ni foam and Pt counter electrode.

	V_{oc} /V	j_{sc} /mA cm^{-2}	FF	η /%
Ni(foam)	0.67	9.62	0.60	3.88
Ni(H_2SO_4)	0.66	11.3	0.59	4.45
Ni(HNO_3)	0.69	10.7	0.64	4.73
Pt	0.74	11.1	0.67	5.57

3.2.2 Camphosulfic acid doped polyaniline (PANI/CSA) electrode

3.2.2.1 Electrochemical properties of PANI/CSA electrode

A counter electrode should have electrocatalytic activity for triiodide reduction. Fig. 3.26(a) demonstrates the comparison of the CV curves for I^-/I_3^- redox about PANI/CSA film on glass and platinized ITO. For this measurement, the 1.2 μm thickness of PANI/CSA film, optimized for the electrocatalytic electrode, was used. According to the CV curves, the PANI/CSA film on glass showed a much higher anodic peak current of 3.7 mA cm^{-2} and cathodic peak current of −1.8 mA cm^{-2} compared to those of platinized ITO. In Fig. 3.26(b), the cathodic current density of PANI/CSA film was less changed after 100 CV cycles. This result suggests that the PANI/CSA film on glass has good reversibility and stability in the I^-/I_3^- redox couple compared to platinized ITO film. Fig. 3.26(c) indicates a linear relationship between the scan rate and cathodic peak current. Thus, the major reaction of iodide reduction on PANI/CSA film was diffusion process.[65] In additions, the twice larger slope of the PANI/CSA film was also attributed to the faster redox reaction, even though this polymer electrode was constructed on a TCO-free substrate. Therefore, it can be ascertained that PANI/CSA coated on TCO-free glass shows superior electrocatalytic activity for triiodide reduction.

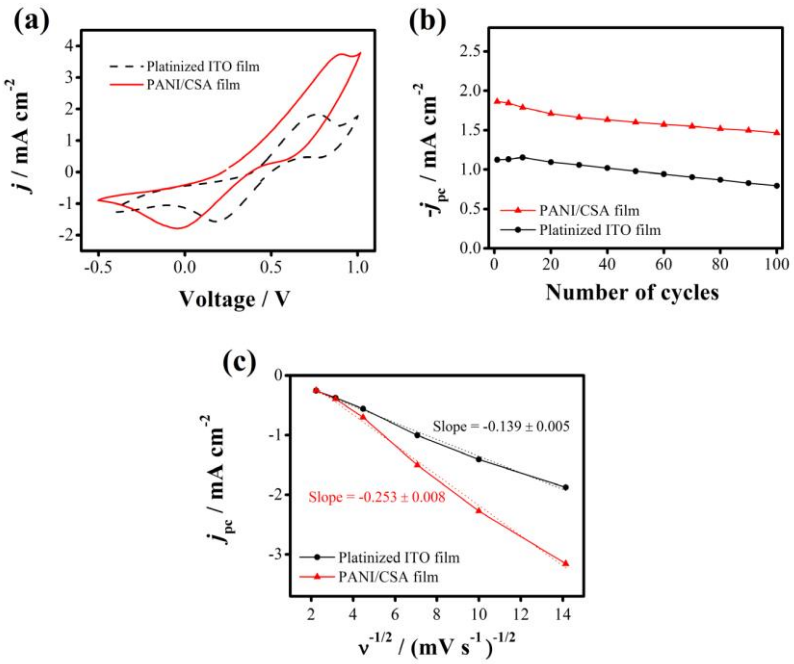

Figure 3.26. The comparison of redox performances of PANI/CSA film and the platinized TCO counter electrode under iodide redox electrolyte; (a) CV curves at 50 mV s^{-1}, (b) the changes in the cathodic peak current density (j_{pc}) during 100 CV cycles, (c) relationship between scan rate and j_{pc}.

3.2.2.2 Optimization of PANI/CSA electrode for counter electrode of DSSC

It was considered that the major factors to improve performance of the PANI/CSA counter electrode were thickness of the film and thermal treatment temperature. Above all, the thickness of the PANI/CSA film strongly affected the performance of the DSSCs. The revolutions per minute (RPM) speed were changed to control the thickness of film. The FE-SEM images of Fig. 3.27(a)-(c) reveal that the thickness of films deposited with 500 RPM, 1000 RPM, and 2000 RPM was 5.1 μm, 1.2 μm, and 488 nm, respectively. The changes in surface morphology with increasing thickness were also presented as described in FE-SEM surface images of Fig. 3.27(d)-(f). The more increasing the thickness of PANI/CSA film, the denser surface of film was obtained. This might lead to the decline in catalytic activity of the counter electrode because the catalytic activity generally depends on the surface area of the catalyst.[33] The mass transport limitations of the electrolyte were also occurred in the thick film. As shown in current transient test (Fig. 3.28(b)), PANI/CSA film deposited by 500 RPM speed was presented this tendency due to thick thickness. The PANI/CSA counter electrodes exhibited higher substrate resistance and lower catalytic activity in EIS curves, Fig 3.29(c), compared to platinized ITO counter electrode (inset plot in Fig. 3.28(c)). The sheet resistance (R_s) was decreased with decreasing the RPM speed due to thicker thickness of PANI/CSA film. The higher charge transfer resistance (R_{ct}) at the counter electrode and electrolyte, high frequency in EIS, was observed with decreasing thickness. To optimize the performance of DSSCs, the rotation speed for spin-coating needs to be fixed to 1000 RPM in order to get best photovoltaic performance as presented in Fig. 3.28(a).

Thermal treatment temperature of the PANI/CSA film was varied to improve DSSC performance. Suitable temperature during the process was an essential to fabricate efficient conducting polymer film because it could affect the surface morphology and conductivity of the film. Fig. 3.29 displays the AFM surface images of PANI/CSA film heated at various temperatures from 50 to 200 ℃. With the exception of the film heated at 100 ℃, the root mean square (RMS) roughness of PANI/CSA film slightly raised from 3.43 to 3.89 nm with increasing thermal treatment temperature as presented in Fig. 3.29(a)-(d). It could be considered that the increment in roughness was attributed to solvent evaporation. m-cresol (b.p. 202.8 ℃) evaporated from the film during the heating step, resulting in the roughness increase of film. This rougher surface provides a larger surface area with potential chances to transfer electrons between the counter electrode and electrolyte.[33,35,73] However, this rough surface could also reduce carrier mobility along the polymer film, which might lead to the decrease of electrocatalytic activity. Indeed, Jung et al. have already reported that the very small change of surface roughness can strongly affect the charge transport property.[74] In additions, the heat treatment temperature affected the CV curves for measuring electrocatalytic activity and electrochromic properties. As presented in the CV curves in Fig. 3.30(a), the PANI/CSA film heated at 100 ℃ shows the highest anodic and cathodic peak current compared to other films which were heated at 50, 150, and 200 ℃. These results suggest that the higher redox current density describes the stronger electrocatalytic activity of PANI/CSA film toward the reduction of the iodide redox couple with thermal treatment at 100 ℃. On the other hands, electrochemical properties decreased significantly when the thermal treatment temperature was over 100 ℃. The PANI/CSA counter electrodes

heated at 50 and 100 ℃ reveal similar electrochromic properties which showed 22 % difference in optical transmittance change between colored/bleach states as indicated in Fig. 3.30(b). However, PANI/CSA counter electrodes heated at 150 and 200 ℃ cannot show electrochromic properties due to the structural change of PANI from half oxidized/half reduced emeraldine base (EB) state to other insulating state.[75,76] Therefore, it could be argued that the PANI/CSA under the condition below 150 ℃ has electrochemical property which can conduct reaction with electrolyte under DSSC system due to the structural deformation.

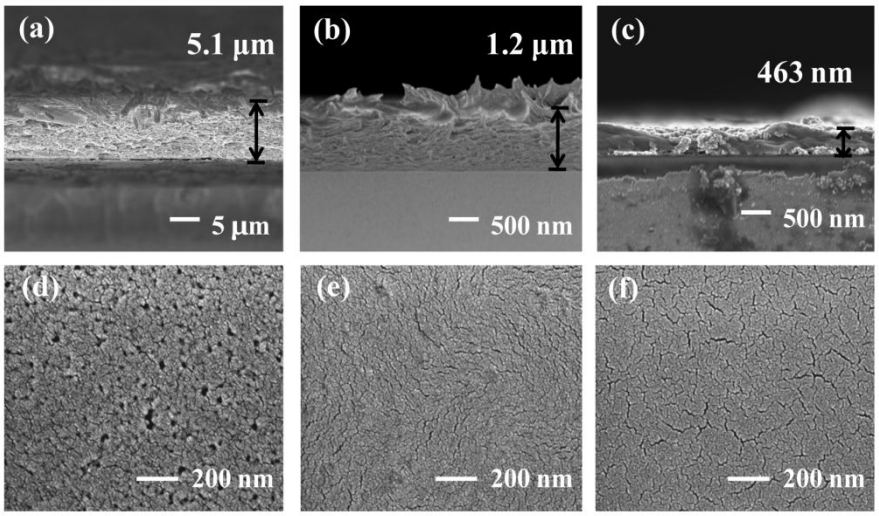

Figure 3.27. FE-SEM images of PANI/CSA films spin-coated with different RPM speed; Cross-sectional images of (a) 500, (b) 1000, and (c) 2000 RPM and suface images of (d) 500, (e) 1000, and (f) 2000 RPM.

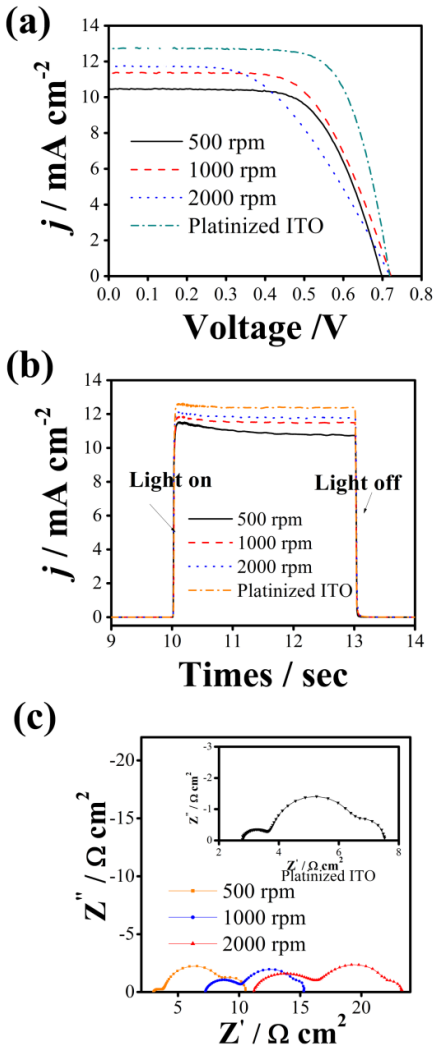

Figure 3.28. The comparison of the DSSC performance of the PANI/CSA counter electrode with various RPM speed and the platinized TCO counter electrode in iodide redox electrolyte; (a) current density–voltage characteristics measurement of the DSSCs, (b) plots of the current transient measurement, and (c) Nyquist plots of the DSSCs from EIS curves.

Table 8. Summary of the *j*–V characteristics of the DSSCs with various PANI/CSA counter electrodes differentiated by controlling RPM speed.

Sample	Thickness (μm)	V_{oc} /V	j_{sc} /mA cm^{-2}	FF	η /%
500 RPM	5.1	0.70	10.50	0.66	4.82
1000 RPM	1.2	0.72	11.37	0.63	5.15
2000 RPM	0.49	0.72	11.72	0.51	4.32
Platinized ITO	-	0.72	12.72	0.71	6.56

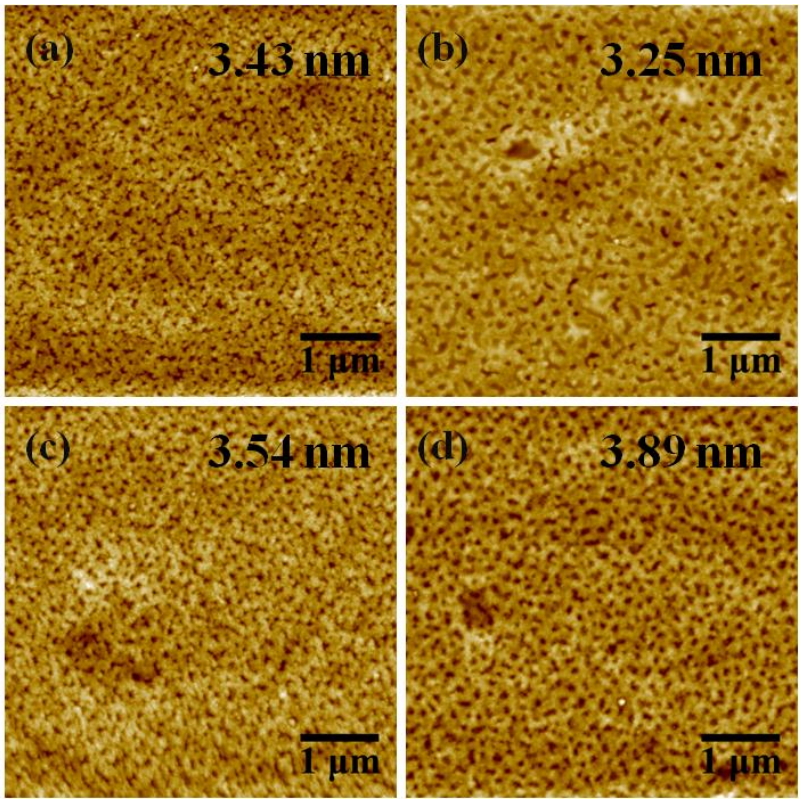

Figure 3.29. AFM images of the PANI/CSA film with different thermal treatment temperature; (a) 50, (b) 100, (c) 150, and (d) 200 °C. RMS roughness values are also described on each figure.

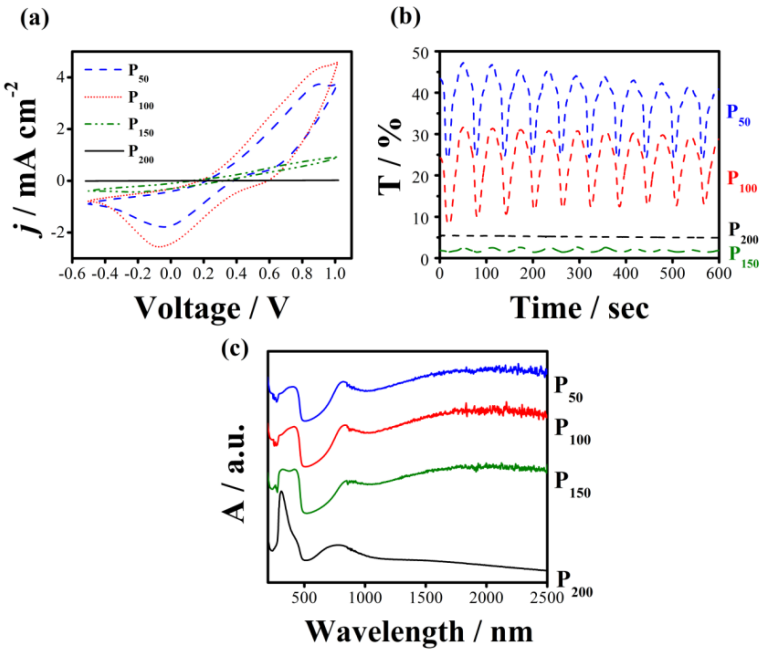

Figure 3.30. Electrochemical properties and optical transmittance changes of PANI/CSA films with different thermal treatment temperatures; (a) CV curves of PANI/CSA films, (b) changes in *in-situ* optical transmittance during continuous potential cycling, and (c) UV-Vis-NIR spectrum of the PANI/CSA film with different thermal treatment temperatures.

3.2.2.3 Application for bifacial DSSC

Fig. 3.31 reveals the comparison of DSSC performances using the counter electrodes with platinized ITO glass and differently heated PANI/CSA films. Table 8 lists performance parameters of DSSCs with these counter electrodes. In Fig. 3.31(b), all kinds of resistance in DSSCs with PANI/CSA counter electrode were higher than that in DSSCs with platinized ITO counter electrode. Therefore, fill factor of DSSCs with PANI/CSA counter electrode was lower than that of DSSCs with platinized ITO counter electrode. The diffusion resistance (W_s) values increased with increasing thermal treatment time. In addition, the lowest value of ohmic series resistance (R_s) and charge transfer resistance at counter electrode/electrolyte interface (R_{ct}) were observed in the film heated at 100 ℃. It is noteworthy that the PANI/CSA film heated at 100 ℃ could be the best functioned counter electrode for DSSCs. Therefore, thermal treatment at 100 ℃ is the optimized condition for efficient PANI/CSA counter electrode of DSSCs. This device exhibited comparable DSSC performance compared to the reference cell, DSSC with the platinized ITO counter electrode which was displayed cell efficiency of 6.56 % as represented in Fig. 3.31(a). The DSSC with PANI/CSA counter electrode presented 84 % of conversion efficiency compared to conventional counter electrode of DSSC. The PANI/CSA film has transparency as shown in inset picture of Fig. 3.31(c). It should be noted that the half-transparent PANI/CSA film could be applied to bifacial DSSC because transparency was crucial for high performance of the bifacial DSSC when the light was cast from the rear side.[57] As described in Fig. 3.31(c), the UV-Vis spectrum of PANI/CSA and platinized ITO counter electrodes after electrolyte injection demonstrate different transmittance patterns. Because

maximum absorption value of dye is 510 nm, the PANI/CSA counter electrode which showed higher transmittance in the range of 450 nm to 650 nm has benefit to light absorption from rear side illumination.[77] It was clearly indicated in IPCE spectrum of Fig. 3.31(d). The DSSC with PANI/CSA counter electrode exhibited higher quantum efficiency from 500 nm to 700 nm. It was noted that the large amount of light could be absorbed on dye due to the complementary absorption properties of PANI film and dye.[77,78] In additions, the improved transparency of PANI/CSA film because of electrochromic properties which was illustrated in Figure 3.32(b) can help to increase light absorption from rear side illumination. Hence, the comparable jsc was observed in DSSC with PANI/CSA counter electrode. As a result, the DSSC with the PANI/CSA film coated on TCO-free glass provided a j_{sc} of 5.44 mA cm^{-2} and cell efficiency of 2.67 % from rear illumination. The DSSC with platinized ITO glass represented a jsc of 5.46 mA cm^{-2} and cell efficiency of 2.86 % under rear illumination. Therefore, it was considered that this comparable efficiency was originated from the effective absorption from front and rear illumination.

The PANI/CSA film had very porous structure as shown in the cross-section FE-SEM image in Figure 3.33(a). This porous electrode was also applied to DSSCs using the cobalt (III/II) redox couple which had slower charge transfer rate than the iodide redox couple. Figure 3.33(b) and (c) depicted the performance in the DSSC device based on the PANI/CSA counter electrode using cobalt electrolyte. The PANI/CSA film heated at 100 ℃, which exhibited the best performance in the electrolyte with the iodide redox couples, was applied to the counter electrode of this device. The reference cell, the

DSSCs with platinized ITO counter electrode, had a j_{sc}, V_{oc}, fill factor and cell efficiency of 8.04 mA cm^{-2}, 0.6 V, 0.62 and 2.97 %, respectively. In contrast, the DSSC with the PANI/CSA film provided a j_{sc}, V_{oc}, fill factor and cell efficiency of 5.22 mA cm^{-2}, 0.56 V, 0.65 and 1.89 %, respectively. Despite the lower current density and cell efficiency compared to the platinized ITO counter electrode, the CSA doped PANI counter electrode also presented comparable cell performance in the cobalt redox electrolyte.

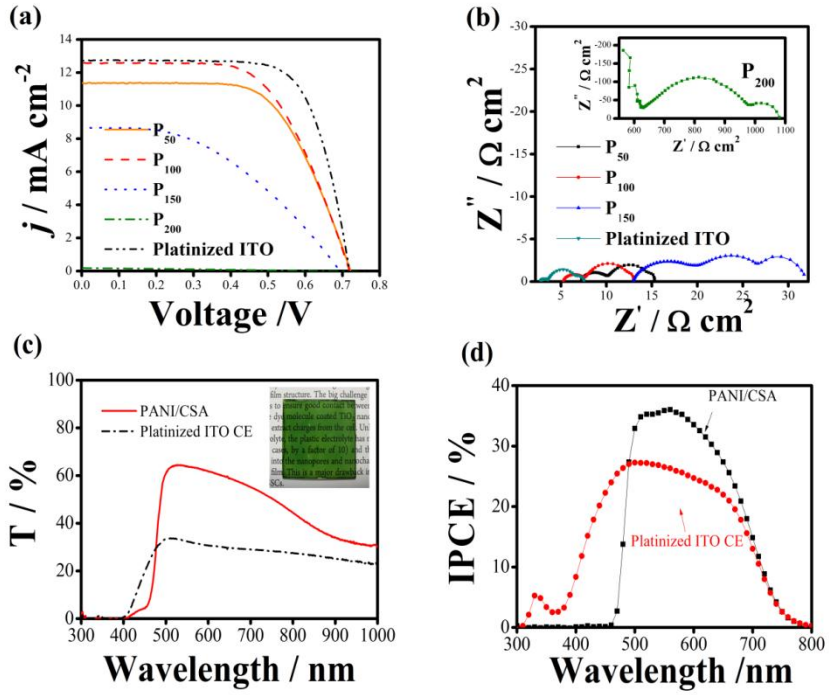

Figure 3.31. (a) Photocurrent–voltage curves of PANI/CSA counter electrodes with different thermal treatment temperatures from front illumination, (b) Nyquist plots of EIS curves, (c) transmittance spectrum after electrolyte injection (inset picture is digital image of transparent PANI/CSA counter electrode), and (d) IPCE spectrum of the DSSCs from rear illumination.

Table 9 Summary of the *j*–V characteristics of the DSSCs with PANI/CSA counter electrodes differentiated by thermal treatment temperature.

	V_{oc} /V	j_{sc} /mA cm^{-2}	FF	η /%
P_{50}	0.72	11.37	0.63	5.15
P_{100}	0.72	12.58	0.61	5.50
P_{150}	0.69	8.67	0.44	2.65
P_{200}	0.65	0.18	0.28	0.03
Platinized ITO	0.72	12.72	0.71	6.56

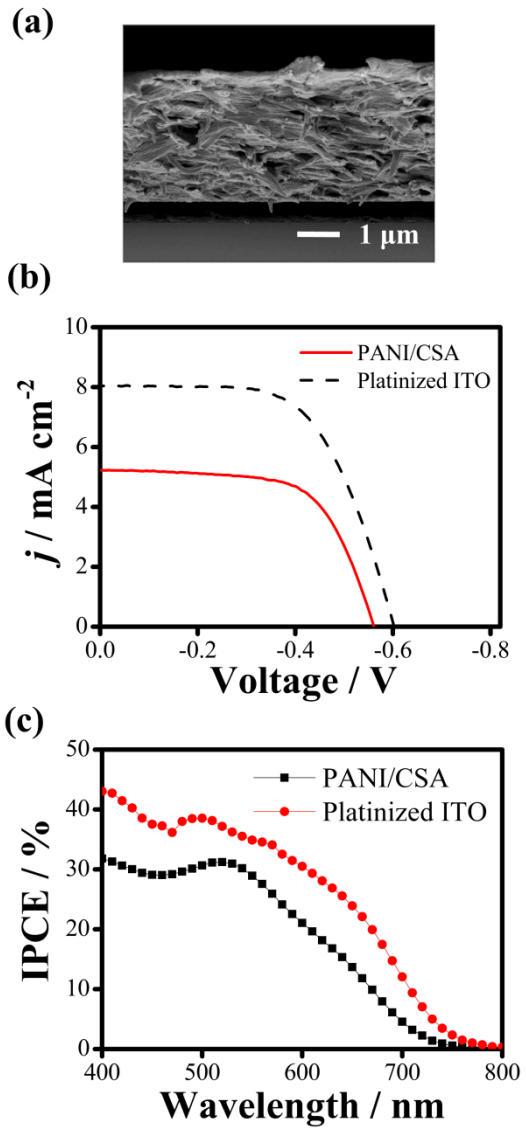

Figure 3.32. Comparison of the performance of the DSSC in the cobalt redox electrolyte; (a) the cross-section image of porous PANI/CSA, (b) current density–voltage characteristics of the DSSCs and (c) IPCE spectra of the DSSCs.

Chapter 4. Conclusions

To obtain cost-effective counter electrode for DSSC, the Pt-free or Pt and TCO-free electrode were used as a counter electrode of DSSC. The conventional platinized TCO glass counter electrodes are used as a catalyst layer and a charge transport layer, respectively. However, Pt is a noble metal with very high cost and TCO electrode was also expensive materials which was the most expensive constituent in DSSC devices.

Firstly, we used the materials with high catalytic activity for I_3^- reduction and rapid charge transport ability to replace Pt layers. The well-ordered inverse opal PEDOT electrode with a PEDOT:PSS filled self-assembled PS opal template was synthesized with novel method and applied as a Pt-free counter electrode for DSSC. Compared to common electrodeposited PEDOT electrode, this inverse opal structured PEDOT electrode was shown improved charge transfer and diffusion of iodide redox electrolyte in various electrochemical measurements due to its porous morphology. Particularly, the improved quantum efficiency at specific wavelength was also observed in IPCE measurement resulted from well-ordered inverse opal structure of the electrode Therefore, we could be successfully applied the inverse opal structured PEDOT electrode as an effective counter electrode for DSSCs. The transition metal nitrides which shown high electrocatalytic activity due to their noble metal-like electronic structures was prepared by sputtering deposition at low-temperature and could be used as a Pt-free counter electrode for DSSC. Because R.F. sputtering deposition did not needed high temperature calcination using ammonia gas to obtain metal nitride, we could be

also obtained Ni nitride flexible electrode which was deposited on ITO/PET substrate. Furthermore, this Ni nitride film shown very thin at nano-scale thickness, this optically transparent Ni nitride counter electrode for bifacial DSSC could be prepared on ITO/PET substrate successfully.

On the other hands, Pt and TCO-free counter electrode was also studied to realize the real cost-effective counter electrode for DSSC. The counter electrode was required electrocatalytic activity to reduce the triiodide to iodide ion and electron conductivity to electron transfer from external circuit to electrode surface. We found out the materials which functioned two things, high catalytic activity for triiodide reduction and rapid charge transport ability in a single layer simultaneously.

The nitrided Ni foam electrode was applied as a Pt and TCO-free counter electrode of DSSC. First of all, the nitrided surface on Ni foam was presented good electrocatalytic activity in iodide redox electrolyte due to their noble metal-like electronic structures as reported in literature. Since this nitrided Ni foam is consisted of three-dimensional interconnected metallic particles, it could be acted as a good electron transfer layer to replace TCO electrode which was typically used as a substrate. In additions, open-pore structures in metal foam can be provided larger surface areas to redox couple in electrolyte and reduced mass transport limitations of the electrolyte in electrode compared to common metal plate. Therefore, the nitrided Ni foam can be a new cost-efficient counter electrode without expensive Pt and TCO. And many various kinds of nitride metal foams could be used as a Pt and TCO-free counter electrode by using this nitridation method in the further works.

Lastly, the camphorsulfonic acid-doped polyaniline (PANI/CSA) electrode was used as a Pt and TCO-free counter electrode for DSSC. The camphorsulfonic acid-doped polyaniline (PANI/CSA)

film was prepared by simple spin-coating deposition and low-tempered treatment. The PANI/CSA spin-coated on normal glass substrate by several optimization process, thickness and heat treated temperature, and it was successfully assembled as a counter electrode of DSSC. The PANI/CSA was a well-known conducting polymer which shown high conductivity and it was provided excellent electrocatalytic ability because π-conjugated polymer superseded Pt as efficient electrocatalyst for iodide reduction reactions. Thus, PANI/CSA film could be presented excellent photovoltaic performance when it applied as a Pt and TCO-free counter electrode of DSSC. Furthermore, the PANI/CSA film which used in this study was illustrated optical transparency and optical transmittance changes with electrochromism properties. Therefore, it demonstrated that the PANI/CSA film can have a promising potential for effective bifacial DSSC with Pt and TCO-free counter electrode.

References

1. M. Grätzel, "Photoelectrochemical cells", *Nature*, **414**, 338 (2001).
2. B. O'Regan and M. Grätzel, *Nature*, **353**, 737 (1991).
3. D. M. Chapin, C. S. Fuller, G. L. Pearson, "A New Silicon p-n Junction Photocell for Converting Solar Radiation into Electrical Power", *J. appl. Phys.*, **25**, 676(1954).
4. A. Yella, H.-W. Lee, H. N. Tsao, C. Yi, A. K. Chandiran, Md.K. Nazeeruddin, E. W.-G. Diau, C.-Y. Yeh, S. M. Zakeeruddin, M. Grätzel, "Porphyrin-Sensitized Solar Cells with Cobalt (II/III)–Based Redox Electrolyte Exceed 12 Percent Efficiency", *Science*, **334**, 629 (2011).
5. M. Grätzel, "Conversion of sunlight to electric power by nanocrystalline dye-sensitized solar cells", *J. Photochem. Photobiol. A*, **164**, 3 (2004).
6. M. Grätzel, "Solar Energy Conversion by Dye-Sensitized Photovoltaic Cells", *Inorg. Chem.*, **44**, 6841 (2005).
7. J.-H. Yum, D. P. Hagberg, S.-J. Moon, K. M. Karlsson, T. Marinado, L. Sun, A. Hagfeldt, M. K. Nazeeruddin, Mi. Grätzel,, "A Light-Resistant Organic Sensitizer for Solar-Cell Applications", *Angew. Chem. Int. Ed.*, **48**, 1576 (2009).
8. Z. Ning Q. Zhang, W. Wua, H. Tian, "Novel iridium complex with carboxyl pyridyl ligand for dye-sensitized solar cells: High fluorescence intensity, high electron injection efficiency?", *J. Organomet. Chem.*, **694**, 2705(2009).
9. T. N. Murakami, M. Grätzel, "Counter electrodes for DSC: Application of functional materials as catalysts", *Inorg. Chim. Acta*, **361**, 572 (2008).

10. J.-Y. Kim, K. J. Lee, S.H. Kang, J. Shin, Y.-E. Sung, "Enhanced Photovoltaic Properties of a cobalt bipyridyl redox electrolyte in dye-sensitized solar cell employing vertically aligned TiO2 nanotube electrodes", *J. Phys. Chem. C*, **115**, 19979 (2011).
11. L. Kavan, J.-H. Yum, M. K. Nazeeruddin, M. Grätzel, "Graphene Nanoplatelet Cathode for Co(III)/(II) Mediated Dye-Sensitized Solar Cells", *ACS Nano*, 5 9171 (2011).
12. H. N. Tsao, J. Burschka, C. Yi, F. Kessler, M. K. Nazeeruddin, M. Grätzel, "Influence of the interfacial charge-transfer resistance at the counter electrode in dye-sensitized solar cells employing cobalt redox shuttles", *Energy Environ. Sci.*, **4**, 4921(2011).
13. Yanhong Luo, Dongmei Li, Qingbo Meng, "Towards Optimization of Materials for Dye-Sensitized Solar Cells", *Adv. Mater.*, **21**, 1 (2009).
14. S. Ahmad, J.-H. Yum, H.-J. Butt, M. K. Nazeeruddin, M. Grätzel, "Efficient Platinum-Free Counter Electrodes for Dye-Sensitized Solar Cell Applications", *ChemPhysChem*, **11**, 2814 (2010).
15. M. Wu, X. Lin, Y. Wang, L. Wang, W. Guo, D. Qi, X. Peng, A. Hagfeldt, M. Grätzel, T. Ma, "Economical Pt-Free Catalysts for Counter Electrodes of Dye-Sensitized Solar Cells", *J. Am. Chem. Soc.*, **134**, 3419 (2008).
16. M. Wu, X. Lin, T. Wang, J. Qiu, T. Ma, "Low-cost dye-sensitized solar cell based on nine kinds of carbon counter electrodes", *Energy Environ. Sci.*, **4**, 2308 (2011).
17. H.-Y. Wang, F.-M. Wang, Y.-Y. Wang, C.-C. Wan, B.-J. Hwang, R. Santhanam, J. Rick, "Electrochemical Formation of Pt Nanoparticles on Multiwalled Carbon Nanotubes: Useful

for Fabricating Electrodes for Use in Dye-Sensitized Solar Cells", *J. Phys. Chem. C*, **115** , 8439 (2011).

18. S. Ahmad, J.-H. Yum, Z. Xianxi, M. Grätzel, H.-J. Butta, M. K. Nazeeruddin, "Dye-sensitized solar cells based on poly (3,4-ethylenedioxythiophene) counter electrode derived from ionic liquids", *J. Mater. Chem.*, **20**, 1654 (2010).
19. G. Yue, J. Wu, Y. Xiao, J. Lin, M. Huang, "Low cost poly(3,4-ethylenedioxythiophene): polystyrenesulfonate/carbon black counter electrode for dye-sensitized solar cells", *Electrochim. Acta*, **67**, 113 (2012).
20. J. Burschka, V. Brault, S. Ahmad, L. Breau, M. K. Nazeeruddin, B. Marsan, S. M. Zakeeruddin, M. Grätzel, "Influence of the counter electrode on the photovoltaic performance of dye-sensitized solar cells using a disulfide/thiolate redox electrolyte", *Energy Environ. Sci.*, **5**, 6089 (2012).
21. M. Wang, A. M. Anghel, B. Marsan, N.-L. Cevey Ha, N. Pootrakulchote, S. M. Zakeeruddin, M. Grätzel, "CoS Supersedes Pt as Efficient Electrocatalyst for Triiodide Reduction in Dye-Sensitized Solar Cells", *J. Am. Chem. Soc.*, **131**, 15976 (2009).
22. G. R. Li, J. Song, G. L. Pan and X. P. Gao, "Highly Pt-like electrocatalytic activity of transition metal nitrides for dye-sensitized solar cells", *Energy Environ. Sci.*, **4**, 1680 (2011).
23. X. Xin, M. He, W. Han, J. Jung, Z. Lin "Low-Cost Copper Zinc Tin Sulfide Counter Electrodes for High-Efficiency Dye-Sensitized Solar Cells", *Angew. Chem. Int. Ed.*, **50** 11739 (2011).

24. B. Yoo, K.-J. Kim, Y. H. Kim, K. Kim, M. J. Ko, W. M. Kim, N.-G. Park, "Titanium nitride thin film as a novel charge collector in TCO-less dye-sensitized solar cell", *J. Mater. Chem.*, **31**, 3077 (2011).

25. G. Veerappan, K. Bojan, S.-W. Rhee. "Sub-micrometer-sized Graphite As a Conducting and Catalytic Counter Electrode for Dye-sensitized Solar Cells", *ACS Appl. Mater. Interfaces*, **3**, 857 (2011).

26. Y. Wang, M. Wu, X. Lin, Z. Shi, A. Hagfeldt, T. Ma, "Several highly efficient catalysts for Pt-free and FTO-free counter electrodes of dye-sensitized solar cells", *J. Mater. Chem.*, **22**, 4009 (2012).

27. K. S. Lee, H. K. Lee, D. H.Wang, N.-G. Park, J. Y. Lee, O. O. Park, J. H. Park, "Dye-sensitized solar cells with Pt- and TCO-free counter electrodes", *Chem. Commun.*, **46**, 4505 (2010).

28. S. H. Park, K.-H. Shina, J.-Y. Kim, S. J. Yoo, K. J. Lee, J. Shin, J. W. Choi, J. Jang, Y.-E. Sung, "The application of camphorsulfonic acid doped polyaniline films prepared on TCO-free glass for counter electrode of bifacial dye-sensitized solar cells", *J. Photochem. Photobiol. A*, **245**, 1 (2012).

29. Q. W. Jiang, G. R. Li, S. Liu, and X. P. Gao, "Surface-Nitrided Nickel with Bifunctional Structure As Low-Cost Counter Electrode for Dye-Sensitized Solar Cells", *J. Phys. Chem. C*, **114**, 13397 (2010).

30. Q. W. Jiang, G. R. Li and X. P. Gao, "Highly ordered TiN nanotube arrays as counter

electrodes for dye-sensitized solar cells", *Chem. Commun.*, 6720 (2009).

31. M. Wu, Q. Zhang, J. Xiao, C. Ma, X. Lin, C. Miao, Y. He, Y. Gao, A. Hagfeldt, T. Ma, "Two flexible counter electrodes based on molybdenum and tungsten nitrides for dye-sensitized solar cells", *J. Mater. Chem.*, **21**, 10761 (2011).
32. A. Hauch, A. Georg, "Diffusion in the electrolyte and charge-transfer reaction at the platinum electrode in dye-sensitized solar cells", *Electrochimi. Acta*, **46**, 3457 (2001).
33. X. Fang, T. Ma, G. Guana, M. Akiyamaa, E. Abe, "Performances characteristics of dye-sensitized solar cells based on counter electrodes with Pt films of different thickness", *J. Photochem. Photobiol. A*, **164**, 179 (2004).
34. X.-Z. Yuan, C. Song, H. Wang, J. Zhang, "Electrochemical Impedance Spectroscopy in PEM Fuel Cells, Fundamentals and Applications", Springer-Verlag, London, (2010).
35. F. F.-Santiago, J. Bisquert, G. G.-Belmonte, G. Boschloo, A. Hagfeldt, "Influence of electrolyte in transport and recombination in dye-sensitized solar cells studied by impedance spectroscopy", *Sol. Energy Mater. Sol. Cells*, **87**, 117 (2005).
36. Y. G. Seo, K. Woo, J. Kim, H. Lee, W. Lee, "Rapid Fabrication of an Inverse Opal TiO_2 Photoelectrodefor DSSC Using a Binary Mixture of TiO_2 Nanoparticles and Polymer Microspheres", *Adv. Funct. Mater.*, 21, 3094 (2011).
37. C. Liu, G. Gao, Y. Zhang, L. Wang, J. Wang, Y. Song, "The Naked-Eye Detection of NH_3–HCl by Polyaniline-Infi ltrated TiO_2 Inverse Opal Photonic Crystals", *Macromol. Rapid Commun.*, **33**, 380 (2012).

38. D.-Y. Kang, Y. Lee, C.-Y. Cho, J. H. Moon, "Inverse Opal Carbons for Counter Electrode of Dye-Sensitized Solar Cells", *Langmuir*, **28**, 2864 (2010).

39. B. C. Tappan, S. A. Steiner III, E. P. Luther, "Nanoporous Metal Foams", *Angew. Chem. Int. Ed.*, **49**, 4544 (2010).

40. A. S. Dimitrov and K. Nagayama, "Continuous Convective Assembling of Fine Particles into Two-Dimensional Arrays on Solid Surfaces", *Langmuir*, **12**, 1303 (1996).

41. L. Santos, P. Martin, J. Ghilane, P.-C. Lacaze, H. Randriamahazaka, L. M.Abrantes, J.-C. Lacroix, "Electrosynthesis of well-organized nanoporous poly(3,4-ethylenedioxythiophene) by nanosphere lithography", *Electrochem. Commun.*, **12**, 872 (2010).

42. L. Liu, S. K. Karuturi, L. T. Su, A. I. Yoong Tok "TiO_2 inverse-opal electrode fabricated by atomic layer deposition for dye-sensitized solar cell applications", *Energy Environ. Sci.*, **4**, 209 (2011).

43. R. B. Pernites, M. J. L. Felipe, E. L. Foster, R. C. Advincula, "Colloidally Templated Two-Dimensional Conducting Polymer Arrays and SAMs: Binary Composition Patterning and Chemistry", *ACS Appl. Mater. Interfaces*, **3**, 817 (2011).

44. F. Jia, W. Sun, J. Zhang, Y. Li, B. Yang, "A facile approach to fabricate three-dimensional ordered macroporous rutile titania at low calcination temperature", *J. Mater. Chem.*, **22**, 2435 (2012).

45. C. M. Elliott, "Indium Tin Oxide Electrodes Modified with Tris(2,2'-bipyridine-4,4'-dicarboxylic acid) Iron(II) and the Catalytic Oxidation of Tris(4,4'-di-tert-

butyl-2,2'-bipyridine) Cobalt(II)", *Langmuir*, 21, 3022 (2005).

46. B. M. Klahr and T. W. Hamann, "Performance Enhancement and Limitations of Cobalt Bipyridyl Redox Shuttles in Dye-Sensitized Solar Cells", *J. Phys. Chem. C*, **113**, 14040 (2009).

47. E. Ramasamy, W. J. Lee, D. Y. Lee, J. S. Song, "Spray coated multi-wall carbon nanotube counter electrode for tri-iodide (I_3^-) reduction in dye-sensitized solar cells", *Electrochem. Commun.*, **10**, 1087 (2008).

48. D. Vempaire, F. Fettar, L. Ortega, F. Pierre, S. Miraglia, A. Sulpice, J. Pelletier, E. K. Hlil, D. Fruchart, "Nonmagnetic thin layers of Ni3N", *J. Appl. Phys.*, **106**, 073911 (2009).

49. G. J. W. R. Dorman and M. Sikkens, "Structure of Reactively Sputtered Nickel Nitride Films", *Thin solid films*, **105**, 251 (1983).

50. M. Kawamura, Y. Abe, K. Sasaki, "Formation process of Ni-N films by reactive sputtering at different substrate temperatures", *Vacuum*, **59**, 721 (2000).

51. Y. Wang, Z.-W. Fu, X.-L. Yue, Q.-Z. Qin, "Electrochemical Reactivity Mechanism of Ni_3N with Lithium", *J. Electrochem. Soc.*, **151**, E162 (2004).

52. H.-M. Kim, J.-S. Park, D. Kim, K. Bae, S. Sohn, "Characteristics of AIN Dielectric Layer for Metal PCB as a Function of Nitrogen Partial Pressure Using RF-Magnetron Sputtering Method", *J. KIEEME*, **10**, 759 (2010).

53. N. Popovic, Z. Bogdanov, B. Goncic, S. S˘trbac, Z. Rakocevic, "Reactively sputtered Ni, Ni(N) and Ni_3N films: Structural, electrical and magnetic properties", *Appl. Surf. Sci.*, **255**,

4027 (2003).

54. X. Zhang, X. Chen, S. Dong, Z. Liu, X. Zhou, J. Yao, S. Pang, H. Xu, Z. Zhang, L. Li, G. Cui, "Hierarchical micro/nano-structured titanium nitride spheres as a highperformance counter electrode for a dye-sensitized solar cell", *J. Mater. Chem.*, **22**, 6067 (2012).

55. M.-H. Yeh, L.-Y. Lin, C.-P. Lee, H.-Y. Wei, C.-Y. Chen, C.-G. Wu, R. Vittal, K.-C. Ho, "A composite catalytic film of PEDOT:PSS/TiN–NPs on a flexible counter-electrode substrate for a dye-sensitized solar cell", *J. Mater. Chem.*, **21**, 19021 (2011).

56. A. Luque, S. Hegedus, Handbook of Photovoltaic Science and Engineering, Wiley, Newyork, 2003.

57. M. Grdeń, M. Alsabet, G. Jerkiewicz, "Surface Science and Electrochemical Analysis of Nickel Foams", *.ACS Appl. Mater. Interfaces*, **4**, 3012 (2012).

58. J. Broiek, F. Grande, J. T. Anderson, A. Keys, "Densitometric Analysis of Body Composition: Revision of Some Quantitative Assumptions", *Annals New York Academy of Sciences*, **110**, 113 (1963).

59. K. A. Hing, S. M. Best W. Bonfield, "Characterization of porous hydroxyapatite", *J. Mater .Sci.: Mater. In Med.*,**10**, 135 (1999).

60. E. C. M. Pennings and W. Grellner, "Precise Nondestructive Determination of the Density of Porous Ceramics", *J. Am. Ceram. Soc.*, **72**, 1268 (1989).

61. H.-G. Yun,Y. Jun, J. Kim, B.-S. Bae, M. G. Kang, "Effect of increased surface area of stainless steel substrates on the efficiency of dye-sensitized solar cells", *Appl. Phys. Lett.*, **93**,

133311 (2008).

62. K.-M. Lee, C.-Y. Hsu, P.-Y. Chen, M. Ikegami, T. Miyasaka, K.-C. Ho, "Highly porous PProDOT-Et_2 film as counter electrode for plastic dye-sensitized solar cells", *Phys. Chem. Chem. Phys.*, **11**, 3375 (2009).
63. S. Cho, S. H. Hwang, C. Kim, J. Jang, "Polyaniline porous counter-electrodes for high performance dye-sensitized solar cells", *J. Mater. Chem.*, **22**, 12164 (2012).
64. Z. Li, B. Ye, X. Hu, X. Ma, X. Zhang, Y. Deng, "Facile electropolymerized-PANI as counter electrode for low cost dye-sensitized solar cell", *Electrochem. Commun.*, **11**, 1768 (2009).
65. Q. Li, J. Wu, Q. Tang, Z. Lan, P. Li, J. Lin, L. Fan, "Application of microporous polyaniline counter electrode for dye-sensitized solar cells", *Electrochem. Commun.*, **10**, 1299 (2008).
66. A. J. Bard and L. R. Faulkner, "Electrochemical Methods: Fundamentals and Applications", John Willy&Sons, INC., Newyork, 2001.
67. K. Miettunen, I. Asghar, X. Ruan, J. Halme, T. Saukkonen, P. Lund, "Stabilization of metal counter electrodes for dye solar cells", *J. Electroanal. Chem.*, **653**, 93 (2011).
68. T. Ma, X. Fang, M. Akiyama, K. Inoue, H. Noma, E. Abe, "Properties of several types of novel counter electrodes for dye-sensitized solar cells", *J. Electroanal. Chem.*, **574**, 77 (2004).
69. X. Fang, T. Ma, M. Akiyama, G. Guan, S. Tsunematsu, E. Abe, "Flexible counter electrodes based on metal sheet and polymer film for dye-sensitized solar cells",

Thin Solid Films, **472**, 242 (2005).

70. M. Toivola, F. Ahlskog, P. Lund, "Industrial sheet metals for nanocrystalline dye-sensitized solar cell structures", *Sol. Energy Mater. Sol. Cells*, **90**, 2881 (2006).
71. Y. J. Kim, M. H. Lee, H. J. Kim, G. Lim, Y. S. Choi, N.-G. Park, K. Kim, W. I. Lee, "Formation of Highly Efficient Dye-Sensitized Solar Cells by Hierarchical Pore Generation with Nanoporous TiO_2 Spheres", *Adv. Mater.*, **21**, 3668 (2009).
72. J. Ferber, and J. Luther, "Computer simulations of light scattering and absorption in dye-sensitized solar cells", *Sol. Energy Mater. Sol. Cells*, **54**, 265 (1998).
73. K. S. Lee, J. H. Yun, Y.-H. Han, J.-H. Yim, N.-G. Park, K. Y. Cho, J. H. Park, "Enhanced light harvesting in dye-sensitized solar cells with highly reflective TCO- and Pt-less counter electrodes", *J. Mater. Chem.*, **21**, 15193 (2011).
74. Y. Jung, R. J. Kline, D. A. Fischer, E. K. Lin, M. Heeney, I. McCulloch, D. M. DeLongchamp, "The Effect of Interfacial Roughness on the Thin Film Morphology and Charge Transport of High-Performance Polythiophenes", *Adv. Funct. Mater.*, **18**, 742 (2008).
75. S. Bhadra, D. Khastgir, N. K. Singhaa, J. H. Lee, "Progress in preparation, processing and applications of polyaniline", *Prog. Polym. Sci.*, **34**, 783 (2009).
76. P. M. S. Monk, R. J. Mortimer, D. R. Rosseinsky, "Electrochromism and electrochromic device", Cambridge university press, Cambridge, 2007.
77. Q. Tai, B. Chen, F. Guo, S. Xu, H. Hu, B. Sebo, X.-Z. Zhao, "In Situ Prepared

Transparent Polyaniline Electrode and Its Application in Bifacial Dye-Sensitized Solar Cells", *ACS Nano*, **5**, 3795 (2011).

78. S. Ameen, M.S. Akhtar, Y.S. Kim, O.-B. Yang, H.-S. Shin, "Sulfamic Acid-Doped Polyaniline Nanofibers Thin Film-Based Counter Electrode: Application in Dye-Sensitized Solar Cells", *J. Phys. Chem. C*, **114**, 4760 (2010).

국문초록

본 연구는 비백금이거나 비백금이며 투명전도성 전극을 동시에 대체할 수 있는 네 가지 저가의 물질을 염료감응형 태양전지의 상대전극으로 적용한 결과들이다. 염료감응형 태양전지의 상대전극으로 일반적으로 사용하는 백금이 증착된 투명 전도성 전극을 대체할 전극으로 쓰이기 위해서는 triiodide의 환원을 위한 높은 촉매 성능과 전자 전달을 빠르게 하기 위한 높은 전도도가 요구된다.

첫 번째로 삼차원으로 잘 정렬된 inverse opal 구조를 가진 PEDOT을 PEDOT:PSS가 채워진 PS opal 템플레이트를 사용하여서 FTO 기판 위에 만들고 이를 염료감응형 태양전지의 비백금 상대전극으로 적용하였다. Inverse opal 구조의 PEDOT 전극은 정렬된 다공성의 구조를 가졌기 때문에 표면적이 커서 triiodide 이온을 환원시키는 전기화학적 활성이 뛰어나며, 또한 특정 파장의 반사율을 증가시키는 inverse opal 구조의 특성을 IPCE 분석에서의 양자 효율의 변화로 확인해 볼 수 있었다. 두 번째로 높은 전기화학적 활성을 가진다는 니켈 나이트라이드 박막을 저온 공정인 R.F. sputtering 방법을 사용해서 ITO/PET 기판에 증착하여 구부림이 가능한 염료감응형 태양전지의 비백금 상대전극으로 적용하였다. 이 실험에서 만들어진 니켈 나이트라이드 박막은 수 나노 미터의 두께를 가지기 때문에 빛이 투과할 수 있는 특성을 가지게 되므로 일반적으로 사용하는 front-

illumination 외에 상대전극을 통한 뒷면에서의 빛 조사가 가능하게 된다. 그러므로 R.F. sputtering을 이용해서 ITO/PET 기판 위에 증착한 니켈 나이트라이드 박막을 상대 전극으로 사용한 염료감응형 태양 전지는 구부림이 가능할 뿐 아니라 양면에서 빛을 효과적으로 사용할 수 있는 양면형 염료감응형 태양전지로 적용될 수 있다.

또한 백금과 더불어서 상대전극에서 사용되는 투명 전도성 유리는 가격적으로 큰 비중을 차지하고 있기 때문에 triiodide 환원 능력을 가지면서 전자의 이동이 원활하게 일어날 수 있도록 전기 전도도를 가진 물질을 백금과 투명전도성 유리를 동시에 대체하도록 하여서 저가의 염료감응형 태양전지의 상대전극을 구현하기 위한 실험을 진행하였다. 우선, 상용으로 판매되는 500 μm 두께를 가지는 니켈 폼을 암모니아 분위기에서 질화 처리하여서 비백금과 투명전도성 기판 제외 염료감응형 태양전지용 상대전극을 만들었다. 질화 처리된 니켈 폼은 표면에 있는 니켈 나이트라이드가 높은 triiodide 환원 능력을 가지고 있고 삼차원으로 네트워크를 이루면서 연결된 내부의 니켈 폼이 높은 전자 전도도를 제공하기 때문에 염료감응형 태양전지로써 큰 이점을 가지고 있다. 또한 니켈 폼 자체가 open-pore 구조를 가지고 있기 때문에 전극 내에서의 전해질의 이동이 아주 손쉽게 일어날 수 있는 장점도 가지고 있다. 마지막으로 camphorsulfonic acid가 2차 도핑된 폴리아닐린 (PANI/CSA)을 일반 유리 기판에 스핀 코팅과 저온의 열처리 공정을 통해서 간단히

제작하여서 염료감응형 태양전지의 상대전극으로 적용하였다. PANI/CSA은 높은 전기화학적 환원 능력과 또한 높은 전기 전도도를 가지고 있다고 알려져 있는 알려진 전도성 고분자로 비백금과 투명전도성 기판 제외 염료감응형 태양전지용 상대전극으로 적합한 물질이다. 상대 전극으로 가장 적합할 수 있도록 두께와 열처리 온도를 최적화해서 염료감응형 태양전지 시스템에 적용한 결과 백금에 버금가는 광변화 효율을 보일 수 있었다. 또한 이 전극은 광학적으로 빛이 투과할 정도로 투명할 뿐만 아니라 빛을 흡수하는 염료와 상보적 색인 초록색을 띄고 있기 때문에 양면형 염료감응형 태양전지로 적용하여 빛을 효과적으로 사용할 수 있다.

주요어: 염료감응형 태양전지, 비백금 상대전극, 비백금과 투명전도성 기판 제외 상대전극, π-conjugated 고분자, 니켈 나이트라이드

학 번: 2009-30242

List of Publications (Sun Ha Park)

1. SCI

1. **Sun Ha Park**, Ju Wan Lim, Sung Jong Yoo, In Young Cha, Yung-Eun Sung, "The Improving Electrochromic Performance of Nickel Oxide Film Using Aqueous N,Ndimethylaminoethanol Solution", *Sol. Energy Mater. Sol. Cells*, **99**, 31 (2012).
2. **Sun Ha Park**, Kyoung-Hwan Shin, Jae-Yup Kim, Sung Jong Yoo, Kyung Jae Lee, Junyoung Shin, Jung Woo Choi, Jyongsik Jang, Yung-Eun Sung, "The application of camphorsulfonic acid doped polyaniline films prepared on TCO-free glass for counter electrode of bifacial dye-sensitized solar cells", *J. Photochem. Photobiol. A*, **245**, 1 (2012).
3. In Young Cha, **Sun Ha Park,** Ju Wan Lim, Sung Jong Yoo, Yung-Eun Sung, "The activation process through a bimodal transmittance state for improving electrochromic performance of nickel oxide thin film", *Sol. Energy Mater. Sol. Cells*, **108**, 22 (2013).
4. Seong Uk Yun, Sung Jong Yoo, Ju Wan Lim, **Sun Ha Park**, In Young Cha, Yung-Eun Sung, "Enhanced Electrochromic Properties of Ir–Ta Oxide Grown, Using a Cosputtering System", *J. Electrochem. Soc.*, **157**, J256 (2010).
5. Sung Jong Yoo, Joon Hyuk Cho, Ju Wan Lim, **Sun Ha Park**, Jyongsik Jang, Yung-Eun Sung, "High contrast ratio and fast switching polymeric electrochromic films based

on water-dispersible polyaniline-poly(4-styrenesulfonate) nanoparticles", *Electrochem. Commun.*, **12**, 164 (2010).

6. Ju Wan Lim, Sung Jong Yoo, **Sun Ha Park**, Seong Uk Yun, Yung-Eun Sung, "High electrochromic performance of co-sputtered vanadium-titanium oxide as a counter electrode", *Sol. Energy Mater. Sol. Cells*, **93**, 2069 (2009).

2. non-SCI

7. **Sun Ha Park**, Sung Jong Yoo, Ju Wan Lim, Seong-Uk Yoon, In Young Cha, Yung-Eun Sung, "Fabrication of Nickel Oxide Thin Film for Lithium Based Electrolyte by Sol-Gel Method and Electrochromic Properties in Lithium Based electrolyte", *J. Korean Electrochem. Soc.*, **12**, 251 (2009).
8. Young-Hoon Chung, **Sun Ha Park**, Hyun-Sik Kim, Yung-Eun Sung, "Layered Nickel-Based Oxides on Partially Oxidized Metallic Copper Foils for Lithium Ion Batteries", *J. Korean Electrochem. Sci. & Tech.*, **2(4)**, 204 (2011).
9. Sung Jong Yoo, Ju Wan Lim, **Sun Ha Park,** Ho Youn Won, Yung-Eun Sung, "Electrochromic Properties of Li^+-Modified Prussian Blue", *J. Korean Electrochem. Soc.*, **10**, 126 (2007).

감사의 글

들뜬 마음으로 입학해서 10 년이 넘는 긴 시간을 다니며 정이 든 서울대학교에서의 생활을 마무리 하고 드디어 새로운 곳으로 나가게 되었습니다. 부족한 제가 모든 학위 과정에 무사히 마침표를 찍을 수 있도록 도움을 주신 많은 분들께 정말로 감사를 드립니다.

석사 과정부터 지금까지 항상 저를 믿고 제가 하는 모든 일에 아낌없는 지원과 격려를 아끼지 않고 연구자의 길로 이끌어주신 성영은 교수님께 먼저 감사 드립니다. 바쁘신 와중에도 제 박사학위 논문을 심사해 주시고 지도해 주신 오승모 교수님, 김대형 교수님, 안광순 교수님, 최희만 교수님께도 깊은 감사를 드립니다.

저와 긴 시간 동안 같이 실험실 생활은 한 광 및 전기화학 연구실 선후배님들께 감사를 드립니다. 연구나 연구실 생활에 대한 조언을 아끼지 않으셨던 유경 언니, 순형 언니, 현식 오빠, 용훈 오빠, 국승 오빠, 태열 오빠, 용훈 오빠, 희영 선배, 백범 오빠, 현서 오빠, 대식 오빠, 예리 언니, 경식 오빠, 남기 선배, 나윤채 박사님, 안철우 박사님께 감사를 드립니다. 그리고 제게 실험과 연구에 대한 지식을 가르쳐 주신 성종 오빠와 재엽 선배, 모자란 선배 밑에서 실험을 같이 하며 고생한 성욱이, 인영이, 정우, 준영, 경재와 선배를 살뜰히 챙기며 졸업을 도와준 진수에게 감사합니다. 또한 저와 공동연구를 하며 제 졸업을 적극적으로 도와주신 방장 옥희

언니에게 감사하고, 또한 광 및 전기화학 에너지 연구실에서 저에게 많은 즐거운 추억 들을 만들어 준 연구실 동료와 후배인 최광현, 정영훈, 유승호, 안민제, 김민건, 정동영, 강윤식, 엄지현, 정진 오빠, 고인환, 김정준, 조민경, 이명재, 이대혁, 김귀룡, 김민형, 이대혁, 강진수, 김애화, 박재혁, 임해나, 영민 오빠, 최지은, 김민정에게 감사하고 건투를 빕니다. 그리고 제가 연구실에서 즐겁게 지낼 수 있도록 여러 가지 도움을 준 조주영씨와 분석에 많은 도움을 준 변누리씨에게도 감사합니다.

저와 공동 연구를 하며 많은 도움을 주신 서울대 장정식 교수님방 신경환씨와 최혜림씨와 최명근씨 외 국민대 신소재 공정 및 평가 실험실 분들께도 이 자리를 빌어서 감사를 전합니다.

제가 힘들 때마다 달려와서 술 한잔과 응원을 보내준 소중한 친구 신희영과 어린 시절부터 항상 함께해 준 미진이와 지혜에게도 고맙습니다.

항상 제가 하고 싶은 일을 하도록 아낌없이 도와주시는 사랑하는 엄마, 아빠께 너무나 감사 드리고 못난 언니를 누구보다 챙겨주는 정하와 석현이에게 너무나 고맙습니다. 마지막으로 대학원 사수이자 연인으로 항상 옆에서 힘을 주고 이끌어주는 주완 오빠에게 감사를 전합니다.

2012년 12월

박 선 하